Analytical expressions for thermophysical properties of solid and liquid tungsten relevant for fusion applications

P. Tolias*, and the EUROfusion MST1 Team[1]

Space and Plasma Physics, Royal Institute of Technology, Stockholm, Sweden

ARTICLE INFO

ABSTRACT

The status of the literature is reviewed for several thermophysical properties of pure solid and liquid tungsten which constitute input for the modelling of intense plasma-surface interaction phenomena that are important for fusion applications. Reliable experimental data are analyzed for the latent heat of fusion, the electrical resistivity, the specific isobaric heat capacity, the thermal conductivity and the mass density from the room temperature up to the boiling point of tungsten as well as for the surface tension and the dynamic viscosity across the liquid state. Analytical expressions of high accuracy are recommended for these thermophysical properties that involved a minimum degree of extrapolations. In particular, extrapolations were only required for the surface tension and viscosity.

1. Introduction

The survivability of the divertor during prolonged repetitive exposures to harsh edge plasma conditions as well as its longevity deep into the nuclear phase are essential for the success of the ITER project and impose stringent requirements on material selection [1]. After the decision that ITER will begin operations with a full tungsten divertor [2], R&D activities worldwide have focused on assessing various sources of mechanical and structural degradation of tungsten plasma-facing components in the hostile fusion reactor environment [3–5]; neutron irradiation effects on mechanical properties, helium irradiation and hydrogen retention effects on the microstructure, thermal shock resistance and thermal fatigue resistance. The dependence of key mechanical properties (ductile to brittle transition temperature, yield strength, fracture toughness) on the fabrication history, the alloying or impurity elements, the metallurgical process and the grain structure is indicative of the complex nature of such investigations [6,7]. As a consequence, the ITER Materials Properties Handbook puts strong emphasis to documenting the mechanical properties of tungsten [8].

Another phenomenon that is crucial for the lifetime of the tungsten divertor is melt layer motion during off-normal or transient events, namely excessively large edge localized modes, vertical displacement events and major disruptions [2]. Melt layer

motion leads to strong modifications of the local surface topology and thus to degradation of power-handling capabilities but can also lead to plasma contamination by high-Z droplets in the case of splashing [9,10]. The numerical modelling of melt motion is based on coupling the Navier–Stokes equations for the liquid metal with the heat conduction equation as well as the current continuity equation and supplementing the system with appropriate boundary conditions dictated by the incident plasma [11–13]. These are the fundamental equations solved in codes such as MEMOS [11,12], where the temperature dependence of the viscosity, surface tension and other thermophysical properties of liquid tungsten constitute a necessary input. In addition, since melting and re-solidification determine the onset and the arrest of macroscopic motion respectively, the thermophysical properties of solid tungsten at elevated temperatures and their behavior at the solid-liquid phase transition are also necessary input. Unfortunately, the ITER Materials Properties Handbook does not provide any information on the thermophysical properties of liquid tungsten and its recommended description of some thermophysical properties of solid tungsten at elevated temperatures is not based on state-of-the-art experimental data [8]. It should also be mentioned that these properties are also essential input for the modelling of tungsten dust transport with codes such as DUSTT [14] and MIGRAINe [15,16] (since tungsten dust should promptly melt in ITER-like edge plasmas and thermionic emission at the liquid phase plays a dominant role in its energy budget [16]) and for the modelling of the interaction of transient plasmas with adhered tung-

---

* Corresponding author.
  E-mail address: tolias@kth.se

[1] See author list of "H. Meyer et al. 2017 Nucl. Fusion 57 102014".

Table 1
Tungsten latent molar heat of fusion according to experiments, theoretical investigations and material handbooks.

Investigators	Reference	Year	Value (kJ/mol)	Details
Lebedev et al.	[20]	1971	54.9	Experimental (resistive pulse heating)
Martynyuk et al.	[21]	1975	54.4	Experimental (resistive pulse heating)
Shaner et al.	[22]	1976	46.0	Experimental (resistive pulse heating)
Seydel et al.	[23]	1979	50.6	Experimental (resistive pulse heating)
Bonnell	[24]	1983	53.0	Experimental (levitation calorimetry)
Arpaci & Frohberg	[25]	1984	50.3	Experimental (levitation calorimetry)
Berthault et al.	[26]	1986	46.7	Experimental (resistive pulse heating)
Senchenko & Sheindlin	[27]	1987	48.0	Experimental (resistive pulse heating)
Hixson & Winkler	[28]	1990	47.8	Experimental (resistive pulse heating)
Kaschnitz et al.	[29]	1990	47.1	Experimental (resistive pulse heating)
McClure & Cezairliyan	[30]	1993	48.7	Experimental (resistive pulse heating)
Pottlacher et al.	[31]	1993	52.4	Experimental (resistive pulse heating)
Kuskova et al.	[32]	1998	45.4	Experimental (resistive pulse heating)
Gustafson	[33]	1985	52.3	Modified experimental input for theory
Grimvall et al.	[34]	1987	52.3	Modified experimental input for theory
Dinsdale	[35]	1991	52.3	SGTE thermochemical database
Lassner & Schubert	[36]	1999	46.0	Handbook of material properties
Lide	[37]	2004	52.3	Handbook of material properties
Martienssen & Warlimont	[38]	2005	52.3	Handbook of material properties
Cardarelli	[39]	2008	52.3	Handbook of material properties
Shabalin	[40]	2014	52.3	Handbook of material properties

sten dust [17] (since wetting is determined by the competition between the spreading and re-solidification rates).

This work is focused on reviewing state-of-the-art measurements of thermophysical properties of pure tungsten from the room temperature up to the boiling point. Complications arising in fusion devices due to strong magnetic fields, intense plasma fluxes, impurity alloying and neutron irradiation are also discussed. The thermophysical properties of interest are the latent heat of fusion, the electrical resistivity, the specific isobaric heat capacity, the thermal conductivity and the mass density (solid and liquid phase) as well as the surface tension and the dynamic viscosity (liquid phase). The objective is to identify and critically evaluate reliable experimental datasets in order to propose accurate analytical expressions for the temperature dependence of these quantities that will standardize their description in the multiple heating, melt layer motion and dust transport codes developed by the fusion community. It has been possible to provide accurate analytical expressions for most properties based solely on experimental data and without the need for any extrapolations. The only exceptions are the surface tension and viscosity of liquid tungsten, where wide extrapolations had to be carried out beyond the melting point, since the only experimental sources on the temperature dependence referred to the under-cooled phase. These extrapolations are based on established empirical expressions that are accurate for non-refractory liquid metals and were cross-checked with rigorous constraints imposed by statistical mechanics. Considering that temperature gradients of the surface tension can drive thermo-capillary flows and that viscosity is responsible for melt motion damping, measurements need to be carried out in the unexplored temperature range, e.g. with levitating drop methods on ground-based laboratories [18] or in microgravity [19].

2. Thermophysical properties of tungsten

2.1. The latent heat of fusion

The difference between the specific enthalpy of the liquid and solid state at the melting phase transition yields the latent heat of fusion. In Table 1, the W latent molar heat of fusion is provided as measured by dedicated experiments [20–32] or as recommended by theoretical investigations [33–35] and material handbooks [36–40]. We point out that the measurement uncertainties in the determination of the heat of fusion with the resistive pulse heating (or

dynamic pulse calorimetry) technique are around 10% [41]. Overall, given these uncertainties, the measurements are well clustered around $\Delta h_{\mathrm{f}} \simeq 50$ kJ/mol, with 52.3 kJ/mol nearly exclusively cited in material handbooks and modelling works.

Some older literature sources recommend a very small value $\Delta h_{\mathrm{f}} \simeq 35.3$ kJ/mol, see for instance Refs. [42,43], which does not seem to be supported by any measurements. Most probably, this value stems from a semi-empirical relation known as Richard's rule [44,45]; By equating the liquid state with the solid state specific Gibbs free energy $g = h - Ts$ at the melting point, we acquire $\Delta h_{\mathrm{f}} = T_{\mathrm{m}} \Delta s_{\mathrm{f}}$. Richard's rule is based on positional disorder arguments and empirical observations, it states that the entropy of fusion is a quasi-universal constant for all metals with an approximate value $\Delta s_{\mathrm{f}} \simeq R$, where $R = N_{\mathrm{A}} k_{\mathrm{B}}$ is the ideal gas constant whose arithmetic value is $R = 8.314$ J/(mol · K). This rule allows the calculation of Δh_{f} with knowledge of the melting temperature T_{m} only. For tungsten, we have $T_{\mathrm{m}} = 3695$ K, which translates to 30.72 kJ/mol. Modified versions of Richard's rule take into account the average value of the entropy of fusion for bcc and fcc metals, which is $\Delta s_{\mathrm{f}} \simeq 1.15R$ [34] and leads to the inaccurate prediction 35.3 kJ/mol. In fact, tungsten is a well-known exception to this entropy rule along with some semi-metals (antimony, bismuth).

2.2. The electrical resistivity

Significance. The role of the electrical resistivity in heat transfer and especially melt motion problems is indirect but can be crucial: (i) It is a key quantity in the determination of the bulk replacement current density $\boldsymbol{J}$, i.e. the current that flows through the conductors as a response to thermionic currents emitted or non-ambipolar plasma currents incident at the surface, which leads to a $\boldsymbol{J} \times \boldsymbol{B}$ force density that is believed to drive macroscopic melt layer motion. This is better illustrated by considering the simplest stationary unmagnetized case, where the replacement current is fully described by the steady state continuity equation $\nabla \cdot \boldsymbol{J} = 0$ and the electrostatic condition $\nabla \times \boldsymbol{E} = 0$ [46]. For the isotropic tungsten, Ohm's law becomes $\boldsymbol{E} = \rho_{\mathrm{el}} \boldsymbol{J}$ and the irrotational equation can be rewritten as $\rho_{\mathrm{el}}(\nabla \times \boldsymbol{J}) + (\nabla \rho_{\mathrm{el}}) \times \boldsymbol{J} = 0$ or by using the chain rule as $\rho_{\mathrm{el}}(\nabla \times \boldsymbol{J}) + (\partial \rho_{\mathrm{el}}/\partial T)(\nabla T \times \boldsymbol{J}) = 0$. The temperature dependence of the resistivity is responsible for the second term that can have a significant effect, since strong temperature gradients are generated by the spatially localized, temporally sharp intra-ELM heat fluxes. (ii) It is proportional to the volumetric resistive

heating caused by the replacement current that is described by the Joule expression $\rho_{el}|J|^2$. (iii) For metals, it is inversely proportional to the thermal conductivity, see Section 2.4 for details.

Solid tungsten. In 1984, Desai and collaborators performed the analysis of all 201 experimental datasets then available for the resistivity of tungsten [47]. A complete dataset covering the temperature range from the neighbourhood of the absolute zero up to 5000 K was synthesized from the most reliable measurements over different temperature intervals. For temperatures below the melting point, we shall be completely based on their analysis. In particular, we shall focus on the temperature range $100 < T(\mathrm{K}) < 3695$. For the purpose of numerical manipulation, polynomial expressions were employed to acquire analytical fits for the electrical resistivity. The *Desai fit* reads as [47]

$$\rho_{el} = \begin{cases} +0.000015 + 7 \times 10^{-7}T^2 + 5.2 \times 10^{-10}T^5 \quad 1\,\mathrm{K} \leq T \leq 40\,\mathrm{K}, \\ +0.14407 - 1.16651 \times 10^{-2}T + 2.41437 \times 10^{-4}T^2 \\ \quad -3.66335 \times 10^{-9}T^4 \quad 40\,\mathrm{K} \leq T \leq 90\,\mathrm{K}, \\ -1.06871 + 2.06884 \times 10^{-2}T + 1.27971 \times 10^{-6}T^2 \\ \quad +8.53101 \times 10^{-9}T^3 - 5.14195 \times 10^{-12}T^4 \quad 90\,\mathrm{K} \leq T \leq 750\,\mathrm{K}, \\ -1.72573 + 2.14350 \times 10^{-2}T + 5.74811 \times 10^{-6}T^2 \\ \quad -1.13698 \times 10^{-9}T^3 + 1.1167 \times 10^{-13}T^4 \quad 750\,\mathrm{K} \leq T \leq 3600\,\mathrm{K}, \end{cases}$$

where ρ_{el} is measured in $10^{-8}\,\Omega\mathrm{m}$ or in $\mu\Omega\mathrm{cm}$. Note that the fitting expression proposed by Desai is continuous at its branch points. The following remarks should be explicitly pointed out: **(i)** The uncertainty in the recommended values employed for the fit is estimated to be $\pm 5\%$ below 100 K, $\pm 3\%$ from 100 to 300 K, $\pm 2\%$ from 300 to 2500 K, $\pm 3\%$ from 2500 up to 3600 K, $\sim \pm 5\%$ in the liquid region. **(ii)** The recommended polynomial fits do not necessarily imply a recommendation for the temperature derivative of the electrical resistivity. **(iii)** A large portion of the experimental datasets analyzed by Desai concern mono-crystalline specimens and many times the orientation of the single crystal is not even mentioned. It can be theoretically expected that the resistivity differences between monocrystalline and polycrystalline tungsten are insignificant, because of the bcc tungsten structure. In fact, this has been observed by Desai by inspecting the data. The synthesized Desai dataset was revisited by White and Minges in 1997 [48]. These authors fitted a fourth-order polynomial to the - corrected for thermal expansion - recommended values in the range $100 < T(\mathrm{K}) < 3600$. The *White–Minges fit* reads as [48]

$$\rho_{el} = -0.9680 + 1.9274 \times 10^{-2}T + 7.8260 \times 10^{-6}T^2 - 1.8517 \\ \times 10^{-9}T^3 + 2.0790 \times 10^{-13}T^4 \quad 100\,\mathrm{K} \leq T \leq 3600\,\mathrm{K},$$

where ρ_{el} is measured in $10^{-8}\,\Omega\mathrm{m}$ or in $\mu\Omega\mathrm{cm}$. This polynomial fit is characterized by a 0.2% rms deviation as well as a maximum deviation of $+0.6\%$ at 150 K and -0.5% at 400 K. Finally, in the MIGRAINe dust dynamics code, the resistivity is also an input, since it is needed for the permittivity model that is employed in the Mie calculation of the emissivity [15]. A polynomial fit has been employed in the MIGRAINe code that is similar to the White–Minges expression. The *MIGRAINe fit* reads as [49]

$$\rho_{el} = +0.000015 + 1.52 \times 10^{-2}T + 1.2003 \times 10^{-5}T^2 - 3.3467 \\ \times 10^{-9}T^3 + 3.7906 \times 10^{-13}T^4 \quad T \leq 3600\,\mathrm{K},$$

where again ρ_{el} is measured in $10^{-8}\,\Omega\mathrm{m}$ or in $\mu\Omega\mathrm{cm}$. A comparison between the resistivities and the resistivity temperature derivatives stemming from the three different fits can be found in Fig. 1. The deviations between the different fits are very small also for the temperature derivative. It is preferable though that the White–Minges fit is employed in future applications and extrapolated up to the actual melting point of 3695 K. The justification for the choice of this fit will be provided in the following paragraph.

Discontinuity at the melting point. The electrical resistivity of all elements has a discontinuity at the melting point. For most liquid metals $\rho_{el}^l > \rho_{el}^s$ but there are few exceptions [50]. Reliable measurements of the W electrical resistivity asymptotically before and after the melting point have been outlined in Table 2. Their mean values are $\langle \rho_{el}^s \rangle \simeq 121\,\mu\Omega\mathrm{cm}$ and $\langle \rho_{el}^l \rangle \simeq 136\,\mu\Omega\mathrm{cm}$. They are very close to the measurements of Seydel & Fucke [51], whose measurements we are going to adopt not only for the discontinuity but also for the liquid state. The extrapolated value of the Desai fit is $\rho_{el}^s \simeq 119\,\mu\Omega\mathrm{cm}$, the extrapolated value of the White-Minges fit is $\rho_{el}^s \simeq 122\,\mu\Omega\mathrm{cm}$ and the extrapolated value of the MIGRAINe fit is $\rho_{el}^s \simeq 122\,\mu\Omega\mathrm{cm}$. Therefore, we conclude that the White–Minges fit (but also the MIGRAINe fit) can be extrapolated from 3600 K to 3695 K with a negligible error.

Liquid tungsten. The electrical resistivity of elemental liquid metals generally exhibits two tendencies [47,50,51]: **(i)** a monotonous increase beyond the melting point at a much slower rate than the solid state increase (e.g. refractory metals such as Ti, V, Mo), **(ii)** a very slow decrease right after the melting point followed by an increase again at a much slower rate than the solid state increase (e.g. the low melting point Zn). Tungsten belongs to the second group [51]. The experimental results have been fitted with a second-order polynomial. The *Seydel–Fucke fit* reads as

$$\rho_{el} = 135 - 1.855 \times 10^{-3}(T - T_m) + 4.420 \\ \times 10^{-6}(T - T_m)^2 \quad T \geq 3695\,\mathrm{K},$$

where ρ_{el} is measured in $10^{-8}\,\Omega\mathrm{m}$. We point out that there are some uncertainties in the temperature measurements due to the lack of data for the temperature dependence of the liquid tungsten emissivity. A constant emissivity has been assumed across the liquid phase, which can be expected to translate from a 5% T-uncertainty near the melting point to a 10% T-uncertainty close to 6000 K. On the other hand, the uncertainties in the resistivity measurements should be $5 - 6\%$. To our knowledge, the only alternative analytical expression for the resistivity of liquid tungsten has been provided by Wilthan et al. [52], see also Refs. [53,54]. Their experiments were performed from 423 K to 5400 K and their measurements were characterized by a 6% resistivity, 4% temperature average uncertainty. A polynomial expression was employed for the fit (including expansion effects). The *Wilthan–Cagran–Pottlacher fit* reads as [52,53]

$$\rho_{el} = 231.3 - 4.585 \times 10^{-2}T + 5.650 \times 10^{-6}T^2 \quad T \geq 3695\,\mathrm{K},$$

where again ρ_{el} is measured in $10^{-8}\,\Omega\mathrm{m}$ or in $\mu\Omega\mathrm{cm}$. From Fig. 2, it is evident that the analytical fits are nearly identical.

Recommended description. The analytical description of the W electrical resistivity consists of employing the White–Minges fit in the temperature range $100 < T(\mathrm{K}) < 3695$ and the Seydel–Fucke fit in the temperature range $3695 < T(\mathrm{K}) < 6000$. The W electrical resistivity is illustrated in Fig. 3. It is worth pointing out that the relative magnitude of the discontinuity of the resistivity at the liquid-solid phase transition is very small, whereas the relative magnitude of the discontinuity of the resistivity temperature derivative is very large (notice also the sign reversal). Finally, we also note that, in the ITER database, a cubic polynomial expression is recommended for the temperature range from 300 to 3300 K [8]. This expression is nearly identical to the Desai, White–Minges and MIGRAINe fits for solid tungsten.

2.3. The specific isobaric heat capacity

Solid tungsten. The fourth and last edition of the NIST-JANAF Thermochemical Tables was published in 1998, but the tungsten data were last reviewed in June 1966 [55]. Measurements from 12 different sources were employed that were published from 1924 up to 1964. Only four of these datasets extend at temperatures beyond 2000 K, whereas five datasets are exclusively focused below the room temperature. The NIST webpage provides a Sho-
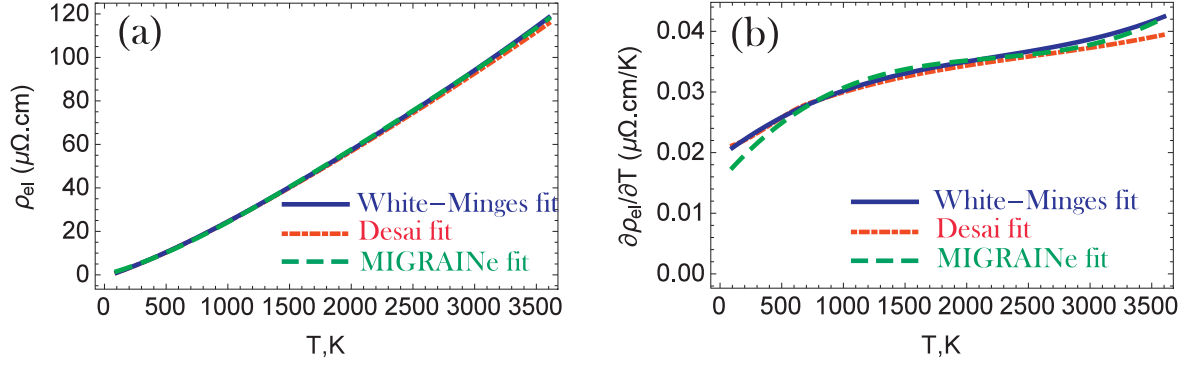
Fig. 1. (a) The solid tungsten resistivity as a function of the temperature according to three empirical analytical expressions. (b) The first temperature derivative of the solid tungsten resistivity as a function of the temperature according to these three analytical expressions.

Table 2

The W electrical resistivity at the solid-liquid phase transition; the values from the solid side $\rho_{el}^s = \rho_{el}(T_m^-)$ and the liquid side $\rho_{el}^l = \rho_{el}(T_m^+)$, as well as the discontinuity magnitude $\Delta\rho_{el} = \rho_{el}^l - \rho_{el}^s$. The first two datasets [20,21] have been corrected for thermal expansion effects following Ref. [47].

| Investigators	Reference	Year	ρ_{el}^s ($\mu\Omega$cm)	ρ_{el}^l ($\mu\Omega$cm)	$\Delta\rho_{el}$ ($\mu\Omega$cm)
Lebedev et al.	[20]	1971	121	127	6
Martynyuk et al.	[21]	1975	118	125	7
Shaner et al.	[22]	1976	118	132	14
Seydel et al.	[23]	1979	120	137	17
Seydel & Fucke	[51]	1980	121	135	14
Desai et al.	[47]	1984	121	131	10
Berthault et al.	[26]	1986	123	138	15
Hixson & Winkler	[28]	1990	126	146	20
Kaschnitz et al.	[29]	1990	118	138	20
Pottlacher et al.	[31]	1993	126	145	19
Kuskova et al.	[32]	1998	120	140	20
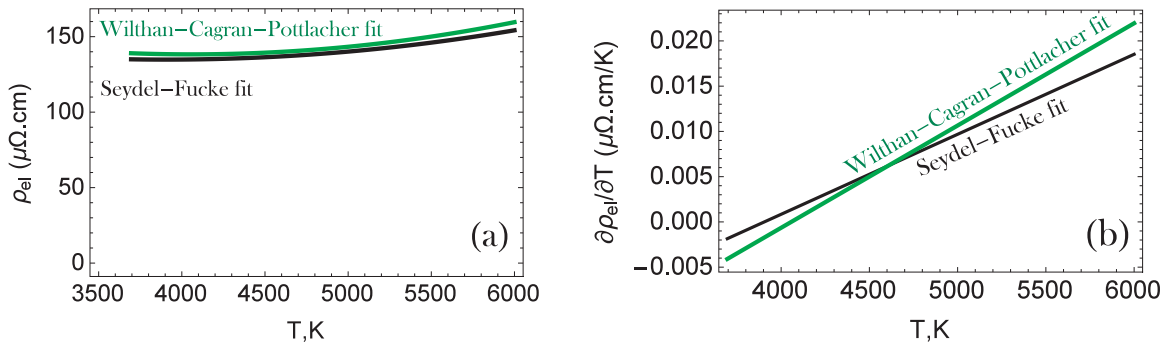
Fig. 2. (a,b) The W electrical resistivity and its first temperature derivative as a function of the temperature across the liquid state according to two empirical analytical expressions.
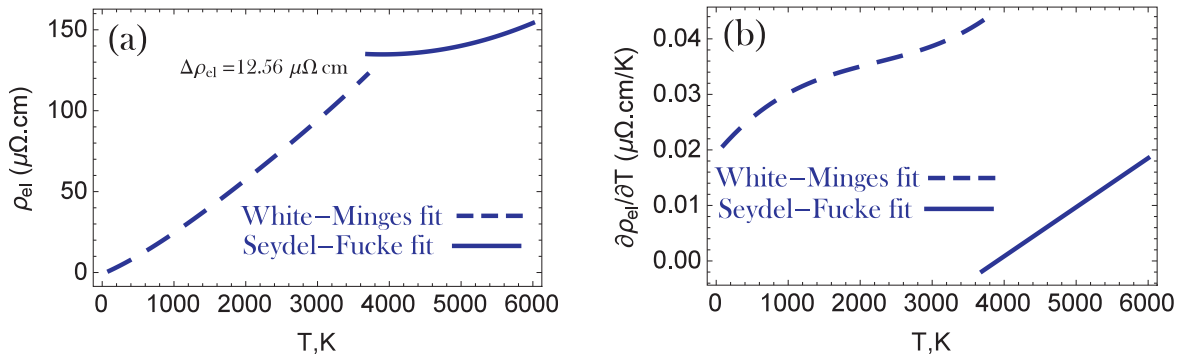

Fig. 3. (a,b) The recommended treatment for the W electrical resistivity and its first temperature derivative for temperatures ranging from 100 up to 6000 K.
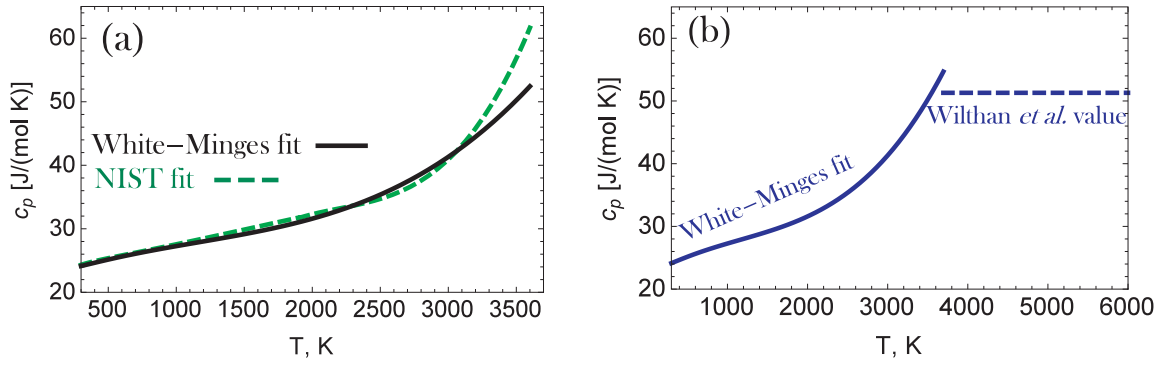
Fig. 4. (a) The W specific isobaric heat capacity in the solid state as a function of the temperature according to two empirical analytical expressions. (b) A complete analytical description of the W specific isobaric heat capacity from 300 to 6000 K by employing the White–Minges fit in the range $300 < T(\mathrm{K}) < 3695$ and the constant value of Wilthan et al. $c_\mathrm{p} = 51.3\,\mathrm{J/(mol\,K)}$ in the range $3695 < T(\mathrm{K}) < 6000$.

mate equation fit in the temperature intervals $298 < T(\mathrm{K}) < 1900$ and $1900 < T(\mathrm{K}) < 3680$. The *NIST fit* reads as [56]

$$c_\mathrm{p} = \begin{cases} +23.9593 + 2.63968 \times 10^{-3}T + 1.25775 \times 10^{-6}T^2 - 2.54642 \\ \quad \times 10^{-10}T^3 - \dfrac{4.8407 \times 10^4}{T^2} \quad 298\,\mathrm{K} \le T \le 1900\,\mathrm{K}, \\ -22.5764 + 9.02798 \times 10^{-2}T - 4.42715 \times 10^{-5}T^2 + 7.17663 \\ \quad \times 10^{-9}T^3 - \dfrac{2.40974 \times 10^7}{T^2} \quad 1900\,\mathrm{K} \le T \le 3680\,\mathrm{K}, \end{cases}$$

where c_p is measured in J/(mol K). In 1997, White and Minges [48] revisited an earlier synthetic dataset of recommended values [57]. In the range above the room temperature, eleven datasets (dating up to 1994) were selected. The *White–Minges fit* reads as [48]

$$c_\mathrm{p} = 21.868372 + 8.068661 \times 10^{-3}T - 3.756196 \times 10^{-6}T^2$$
$$+ 1.075862 \times 10^{-9}T^3 + \frac{1.406637 \times 10^4}{T^2} \quad 300\,\mathrm{K} \le T \le 3400\,\mathrm{K},$$

where c_p is measured in J/(mol K). This fit is characterized by a 1.1% rms deviation, the deviation from the mean is generally less than 1% below 1000 K and less than 2.5% above 1000 K. We point out that there are two misprints in the fitting expression as quoted in the original work [48]. As illustrated in Fig. 4a, the two expressions begin to strongly diverge above 2900 K; the high temperature measurements employed in the NIST fit are far less reliable.

Liquid tungsten. Measurements on free-electron-like elemental metals with low melting points [44] as well as recent experiments on elemental transition metals [31,54] indicate that the enthalpy of liquid metals increases nearly linearly with the temperature over a wide range. In the case of liquid tungsten, the literature consensus is also that the enthalpy at constant pressure is a linear function of the temperature. This implies a constant isobaric heat capacity, courtesy of $(\partial H/\partial T)_P = C_\mathrm{p}$. Thus, also the specific isobaric heat capacity $c_\mathrm{p} = \partial C_\mathrm{p}/\partial m$ should be constant. However, there is a disagreement concerning the exact value: **(i)** The NIST-JANAF recommended value is $c_\mathrm{p} = 35.564\,\mathrm{J/(mol\,K)}$. It is very outdated, being based on experiments that were carried out prior to 1961, *i.e.* many years before the dynamic pulse calorimetry or levitation calorimetry methods were developed. Unfortunately, this value is quoted in material property handbooks [36]. **(ii)** More reliable measurements provide values that are clustered around $c_\mathrm{p} = 52\,\mathrm{J/(mol\,K)}$. We have $c_\mathrm{p} = 51.8\,\mathrm{J/(mol\,K)}$ [22], $c_\mathrm{p} = 57.0\,\mathrm{J/(mol\,K)}$ [23], $c_\mathrm{p} = 55.1\,\mathrm{J/(mol\,K)}$ [26], $c_\mathrm{p} = 48.2\,\mathrm{J/(mol\,K)}$ [28], $c_\mathrm{p} = 56.1\,\mathrm{J/(mol\,K)}$ [29], $c_\mathrm{p} = 52.9\,\mathrm{J/(mol\,K)}$ [31], $c_\mathrm{p} = 53.7\,\mathrm{J/(mol\,K)}$ [32]. Such deviations are justified in view of the fact that c_p is not directly obtained by the measurements but after post-processing (graphical determination from the slope of the enthalpy versus temperature trace) and thus is subject to

an uncertainty of around 10% [41]. **(iii)** To our knowledge, the most contemporary experiments are those performed by Wilthan et al. [52] in 2005, who performed measurements up to 5400 K and found a constant liquid W $c_\mathrm{p} = 51.3\,\mathrm{J/(mol\,K)}$ - 8% uncertainty - that we shall adopt.

Recommended description. (i) A complete analytical description of the tungsten specific isobaric heat capacity can be constructed by combining the White–Minges fit in the temperature range $300 < T(\mathrm{K}) < 3695$ and the constant value $c_\mathrm{p} = 51.3\,\mathrm{J/(mol\,K)}$ in the temperature range $3695 < T(\mathrm{K}) < 6000$. See also Fig. 4b. This implies that the White–Minges fit needs to be extrapolated in the temperature range $3400 < T(\mathrm{K}) < 3695$. This leads to $c_\mathrm{p}^\mathrm{s} \simeq 54.7\,\mathrm{J/(mol\,K)}$ and thus to $\Delta c_\mathrm{p} \simeq 3.4\,\mathrm{J/(mol\,K)}$. However, as can be observed in Fig. 4a, the heat capacity starts rapidly increasing at high temperatures, which implies that any extrapolation can lead to significant errors. **(ii)** Wilthan et al. have also provided an analytical fit for the tungsten specific enthalpy in the range $2300 < T(\mathrm{K}) < 3687$ [52]. Their fit reads as $h(T) = 83.342 + 0.011T + 3.576 \times 10^{-5}T^2$ (kJ/kg) with 4% measurement uncertainty. It would be certainly preferable that the heat capacity was calculated from the local slopes of the experimental data, but here we have to differentiate the above fitting expression, which yields $c_\mathrm{p} = 11 + 7.152 \times 10^{-2}T$ [J/(kg K)] or $c_\mathrm{p} = 2.022 + 1.315 \times 10^{-2}T$ [J/(mol K)]. Therefore, we have $c_\mathrm{p}^\mathrm{s} \simeq 50.6\,\mathrm{J/(mol\,K)}$ and thus $\Delta c_\mathrm{p} \simeq -0.7\,\mathrm{J/(mol\,K)}$. **(iii)** Both results are physically acceptable; At the melting point, the difference in the heat capacity of metals between the solid and the liquid phases is rather small and it can be of either sign [44,58]. **(iv)** In their common range of validity, the fits agree exceptionally well, see Fig. 5a, but they start diverging at both the interval endpoints. It is preferable to avoid any extrapolations and employ both fits. We shall first calculate their highest temperature intersection point, which is $T \simeq 3080\,\mathrm{K}$. This allows us to connect the two fitting expressions in a continuous manner. The recommended description has the form

$$c_\mathrm{p} = \begin{cases} 21.868372 + 8.068661 \times 10^{-3}T - 3.756196 \times 10^{-6}T^2 \\ \quad + 1.075862 \times 10^{-9}T^3 + \dfrac{1.406637 \times 10^4}{T^2} \quad 300\,\mathrm{K} \le T \le 3080\,\mathrm{K} \\ 2.022 + 1.315 \times 10^{-2}T \quad 3080\,\mathrm{K} \le T \le 3695\,\mathrm{K} \\ 51.3 \quad T \ge 3695\,\mathrm{K} \end{cases}$$

where c_p is again measured in J/(mol K). The recommended analytical description is illustrated in Fig. 5b.

Comparison with the fusion literature. *In the ITER database*; a quadratic polynomial expression is recommended which is valid in the range $273 - 3100\,\mathrm{K}$ [8]. It originates from fitting to a synthetic dataset, whose high temperature part is heavily based on measurements provided in the classic 1971 compendium by Touloukian [59]. As illustrated in Fig. 6a, the ITER recommendation
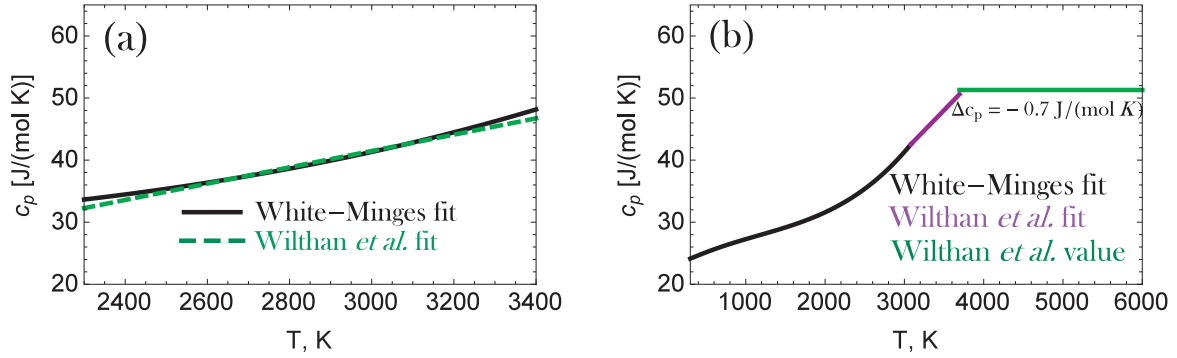
Fig. 5. (a) The specific isobaric heat capacity of solid state tungsten in the range $2300 < T(K) < 3400$ according to two empirical analytical expressions. (b) The complete recommended analytical description of the W specific isobaric heat capacity from 300 to 6000 K.
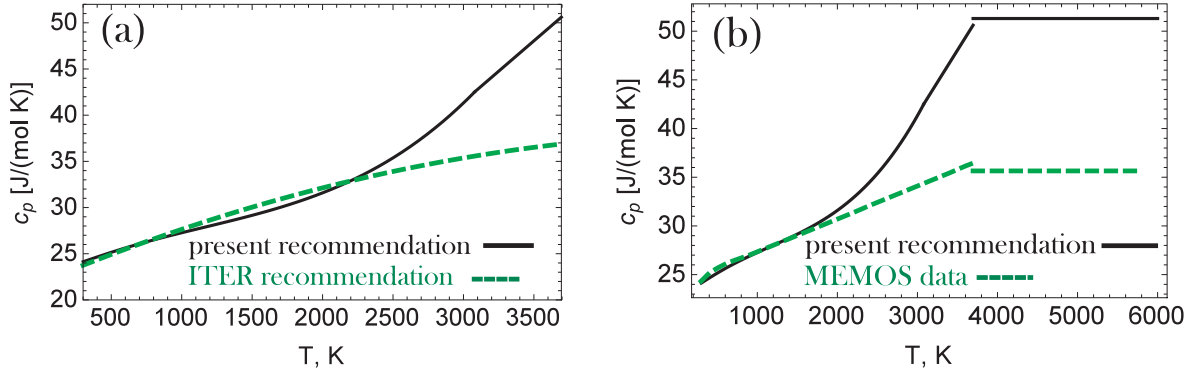

Fig. 6. (a) Comparison of the recommended analytical description of the W specific isobaric heat capacity with the ITER database recommendation in the temperature range from 300 to 3695 K. (b) Comparison of the recommended analytical description of the W specific isobaric heat capacity with the MEMOS code description in the temperature range from 300 to 6000 K.

is outdated. The underestimations of the heat capacity start from 2200 K and monotonically increase up to 3100 K. In the extrapolated range $3100 - 3695$ K, the situation becomes progressively worse with the underestimation reaching 40% close to the phase transition. *In the MEMOS code*; a dataset based on Touloukian's compendium is implemented for interpolations in the solid state, whereas the constant NIST-JANAF value of $c_p = 35.564$ J/(mol K) is employed for the liquid state [11]. As evident from Fig. 6b, in MEMOS, the heat capacity is underestimated from 1700 K with the deviations approaching $\sim 40\%$ from above ~ 3000 K and across the entire liquid state. *Consequences*; Underestimation of the heat capacity translates to overestimation of the temperature in the MEMOS simulations compared to the experiments, which could be erroneously attributed to a decreased heat flux incidence from the inter-ELM and intra-ELM plasma. Furthermore, this implies an overestimation of the melt layer depth and a premature initiation of bulk melting during prolonged exposures.

2.4. The thermal conductivity

Preliminaries. (i) In condensed matter, heat transfer is mediated by the collisional transport of valence electrons and lattice waves. In metals, the electron contribution dominates over the phonon contribution (which is limited by Umklapp processes) with the exception of samples with high impurity concentration at very low temperatures [60,61]. Due to the fact that the valence electrons are responsible for both charge and heat transfer in metals, a proportionality between the thermal conductivity and the electrical conductivity can be expected. This is expressed by the so-called Wiedemann–Franz law that can be derived within Sommerfeld's free-electron theory and the Lorentz gas approximation, it reads as $k = \left[(\pi^2 k_b^2)/(3e^2) \right][T/\rho_{el}]$ [60–62]. The term in

brackets is known as the Lorenz number and its nominal value is $L_0 = 2.443 \times 10^{-8}$ WΩK^{-2}. **(ii)** The resistance to heat transfer by electrons originates from collisions with phonons and collisions with atomic impurities, crystal boundaries, lattice imperfections. The coupling between these collisional contributions is limited, which implies an additivity that is expressed by Matthiessen's rule. However, with the exception of extreme cases where the impurity/imperfection concentration is very large, electron-phonon collisions dominate already from the room temperature [61]. Thus, for our temperature range of interest, the thermal conductivity can be expected to be weakly dependent on crystalline structure details.

Solid tungsten. *In 1972*; Ho, Powell and Liley provided recommended and estimated thermal conductivity values for elements with atomic numbers up to $Z = 105$ [63,64]. Datasets were synthesized for 82 elements after careful analysis of 5200 different sets of experimental measurements. Their recommended tungsten dataset will not be employed for the determination of the fitting expression but will be employed for comparison with our recommended treatment. *In 1984*; Hust and Lankford critically analyzed all literature data on the thermal conductivity of four reference metals (aluminium, copper, iron, tungsten) for temperatures up to melting and provided analytical fits based on theoretical descriptions [65]. For $T > 200$ K, the uncertainty in their proposed values was estimated to be 5%. We note that their analysis was later closely followed by White and Minges [48]. Intricate details of their analysis as well as their utilization of the residual resistivity ratio will not be discussed here, since they are important for the low temperature part of the thermal conductivity ($\lesssim 100$ K), which is not relevant for fusion applications. They utilized 13 datasets for their fit, which contain measurements from 2 K up to 3000 K (only 4 datasets refer to $T \geq 2000$ K). The basic ingredients of the
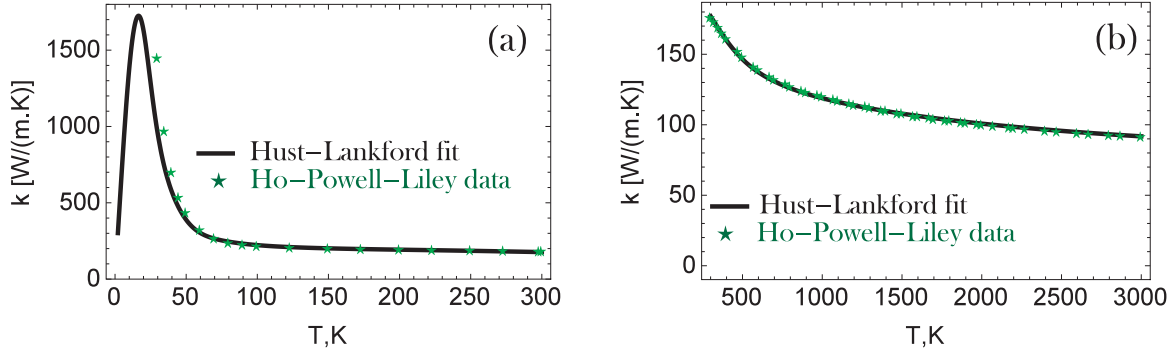
Fig. 7. The solid tungsten thermal conductivity. Comparison of the Hust–Lankford analytical fit [65] with the Ho–Powell–Liley [63,64] recommended dataset in (a) the low temperature interval $2 < T(K) < 300$, where the deviations rapidly increase as $T < 40$ K, (b) the intermediate and high temperature interval $300 < T(K) < 3000$, where the agreement is excellent. The uncertainties in the Ho–Powell–Liley recommendations are 3% in the $300 - 1500$ K and 5% in the $1500 - 3000$ K range [63,64].

Hust–Lankford fit for tungsten are the electron-defect interaction term W_o ($\propto T^{-1}$), the electron-phonon interaction term W_i (approximately $\propto T^2$), the interaction coupling term W_{io} (nearly zero for tungsten) and the residual deviation term W_c, which are combined to provide the thermal conductivity in a manner reminiscent of Matthiessen's rule. The analytical expressions and their connection to the thermal conductivity read as [65]

$$W_c(T) = -0.00085 \ln\left(\frac{T}{130}\right) \exp\left\{-\left[\ln\left(\frac{T}{230}\right)\frac{1}{0.7}\right]^2\right\}$$

$$+0.00015 \exp\left\{-\left[\ln\left(\frac{T}{3500}\right)\frac{1}{0.8}\right]^2\right\}$$

$$+0.0006 \ln\left(\frac{T}{90}\right) \exp\left\{-\left[\ln\left(\frac{T}{80}\right)\frac{1}{0.4}\right]^2\right\}$$

$$+0.0003 \ln\left(\frac{T}{24}\right) \exp\left\{-\left[\ln\left(\frac{T}{33}\right)\frac{1}{0.5}\right]^2\right\},$$

$$W_i(T) = \frac{P_1 T^{P_2}}{1 + P_1 P_3 T^{(P_2+P_4)} \exp\left[-(P_5/T)^{P_6}\right]}, \quad W_o(T) = \frac{\beta}{T},$$

$$k = \frac{1}{W_o(T) + W_i(T) + W_c(T)}.$$

The constant β has been chosen to correspond to a residual resistivity ratio of 300, whereas the P_i parameters were determined by least square fits of the combined dataset. Their arithmetic values are [65]

$$\beta = 0.006626, \quad P_1 = 31.70 \times 10^{-8}, \quad P_2 = 2.29, \quad P_3 = 541.3,$$

$$P_4 = -0.22, \quad P_5 = 69.94, \quad P_6 = 3.557.$$

Surprisingly, a comparison of the fit with the tabulated values reveals deviations below 90 K. This can either originate from misprints in the residual deviation W_c or from improper rounding-off of the least square coefficients. Since these deviations lie well below our temperature range of interest, we have not pursued this issue further. For completeness, the functional form of the tungsten thermal conductivity according to the Hust–Lankford fit is illustrated in Fig. 7. The plot covers the full temperature range of validity, $2 < T(K) < 3000$, but the fit will only be utilized in the temperature range $300 < T(K) < 3000$. In the latter range, the comparison with the Ho–Powell–Liley recommended dataset reveals a remarkable agreement. On the other hand, in the low temperature range, there are very strong deviations below 40 K (exceeding by far the selected plot scale). The emergence of these deviations is theoretically expected; they are a direct consequence of the electron-defect interaction term, which becomes dominant at very low temperatures and is a very sensitive function of the sample purity [60]. The Hust–Lankford fitting function is relatively cumbersome for numerical simulations. Its complexity stems from the low temperature maximum of the thermal conductivity, whose position lies well below fusion regimes of interest. An alternative empirical expression has been found by digitizing the Hust–Lankford fitting function with sampling steps of 50 K from 300 K to 3700 K and by least squares fitting the emerging dataset to the Shomate equation. This *modified Hust–Lankford fit* reads as

$$k = 149.441 - 45.466 \times 10^{-3}T + 13.193 \times 10^{-6}T^2 - 1.484$$

$$\times 10^{-9}T^3 + \frac{3.866 \times 10^6}{T^2},$$

where k is measured in W/(m K). The mean value of the absolute relative fitting error is 0.4%, its maximum is 1.6%.

Liquid tungsten. **(i)** Experimental techniques that directly measure the thermal conductivity are based on formulas that are valid when heat conduction is the only viable mode of heat transfer. Their applicability to high temperature liquid metals such as tungsten is limited due to the increasing importance of convective and radiative heat transfer [66]. **(ii)** Experimental techniques that measure the thermal diffusivity $\alpha = k/(\rho_m c_p)$ can lead to the evaluation of the thermal conductivity [66]. However, post-processing requires the simultaneous knowledge of the mass density and the heat capacity, thus the resulting measurement uncertainty can be large. **(iii)** Experimental techniques that measure the electrical resistivity ρ_{el} can also lead to the evaluation of the thermal conductivity [41,50,66,67]. The connecting relation is the Wiedemann–Franz law, $k = L_0 T/\rho_{el}$ with $L_0 = 2.443 \times 10^{-8}$ WΩK^{-2} the nominal Lorenz number. In this manner, the abundance of liquid tungsten resistivity data, acquired by dynamic pulse calorimetry, can be translated to thermal conductivity data. The use of the $\rho_{el}(T)$ fitting expressions with the Wiedemann–Franz law can lead to the propagation of numerical errors. Therefore, when possible, it is preferable that first each resistivity data point is translated to thermal conductivity and that afterwards curve fitting takes place. This procedure has been followed for the Seydel and Fucke measurements [51]. In the original publication, the authors only provide the fitting expression for the resistivity, but their resistivity data have been presented in graphical form in Ref.[52]. The data have been extracted with the aid of software, they are represented by the average of three different extractions in order to avoid errors due to axis mismatch. The measurements consist of 13 datapoints from the melting temperature up to 6000 K and have been fitted with a quadratic polynomial. The *Seydel–Fucke fit* reads as

$$k = 66.6212 + 0.02086(T - T_m) - 3.7585 \times 10^{-6}(T - T_m)^2 \quad 3695 \text{ K}$$

$$\leq T \leq 6000 \text{ K},$$

where k is measured in W/(m K). The mean value of the absolute relative fitting error is 0.25%, see also Fig. 8a. Let us compare with
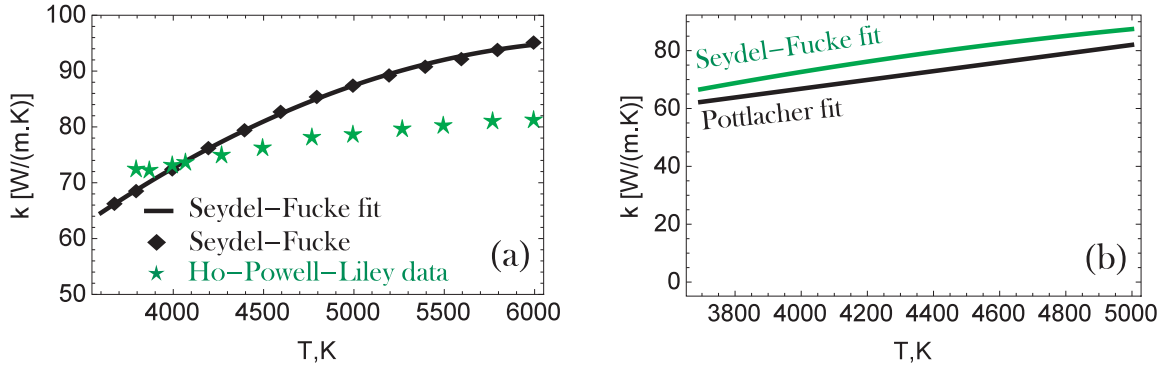
Fig. 8. (a) The liquid tungsten thermal conductivity in the range $3695 < T(K) < 6000$. The data of Seydel–Fucke [51,52] (together with a quadratic fit) compared with the provisional values provided by Ho–Powell–Liley [63,64]. (b) The thermal conductivity of liquid tungsten in the temperature range $3695 < T(K) < 5000$ according to two empirical analytical expressions.
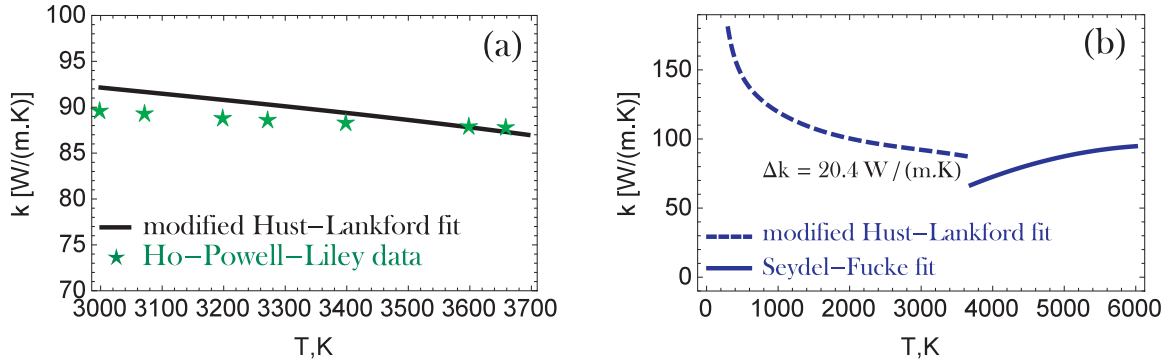

Fig. 9. (a) Extrapolation of the modified Hust–Lankford fit in the temperature range $3000 < T(K) < 3695$ and comparison with the values recommended by Ho–Powell–Liley [63,64]. (b) The complete recommended analytical description of the W thermal conductivity from 300 to 6000 K.

the measurements of Pottlacher from melting up to 5000 K [68]. The *Pottlacher fit* reads as [68]

$$k = 6.24242 + 0.01515T \quad 3695\,\mathrm{K} \leq T \leq 5000\,\mathrm{K},$$

where k is measured in W/(m K). We point out that typical uncertainties in the indirect determination of the thermal conductivity with dynamic pulse calorimetry are $\sim 12\%$ [41,67]. The two fitting functions are plotted in Fig. 8b, in their common domain of definition. The deviations are acceptable being $< 7\%$. Moreover, we note that the Seydel–Fucke experiments are in better agreement with other recent measurements [69]. Finally, it is worth mentioning that Ho–Powell–Liley provide provisional values for the thermal conductivity of tungsten over its entire liquid range, from the melting up to the critical point [63,64]. These values were estimated with the phenomenological theory of Grosse, which is based on an empirical hyperbolic relation for the electrical conductivity of liquid metals [70,71]. As illustrated in Fig. 8a and expected due to the oversimplified theoretical analysis, these provisional values are not accurate.

Recommended description. In order to complete the description, it is necessary to verify that the extrapolation of the modified Hust–Lankford fit in the temperature range $3000 < T(K) < 3695$ is viable. (i) We have confirmed that the extrapolated values lie very close to the Ho–Powell–Liley recommended dataset [63,64], which features seven data-points in this range, see Fig. 9a. (ii) We have performed a comparison with the thermal conductivity resulting from the combination of the White–Minges fit for the electrical resistivity [48] with the Wiedemann–Franz law. The agreement was satisfactory. We also note that the two curves overlap when employing $L_{\mathrm{eff}} = 1.185 L_0$ for the effective Lorenz number. (iii) Overall, the recommended description comprises of the modified Hust–Lankford fit in the temperature range $300 < T(K) < 3695$ and

the Seydel–Fucke fit in the temperature range $3695 < T(K) < 6000$. See Fig. 9b for an illustration. (iv) From the above, we have $k^s \simeq 87.0\,\mathrm{W/(m\ K)}$ and $k^l \simeq 66.6\,\mathrm{W/(m\ K)}$. The resulting discontinuity at the liquid-solid phase transition is $\Delta k \simeq 20.4\,\mathrm{W/(m\ K)}$. The large relative magnitude of the discontinuity and the fact that $k^s > k^l$ agrees with results from other refractory metals [66].

Comparison with the fusion literature. *In the ITER database*; a cubic polynomial expression is recommended which is valid in the range $273 - 3653\,\mathrm{K}$ [8]. It originates from fitting to a synthetic dataset, whose high temperature part is heavily based on the recommended dataset provided in the classic 1970 compendium by Touloukian [72]. As illustrated in Fig. 10a, the ITER fit agrees well with our recommended description from the room temperature up to the melting point. However, the ITER fit is characterized by two rather un-physical inflection points, the local sign switching of $\partial k/\partial T$ might influence thermal modelling due to the $\nabla \cdot (k\nabla T)$ term in the heat conduction equation. *In the MEMOS code*; Touloukian's recommended dataset is implemented for interpolations in the solid state, whereas the Ho–Powell–Liley provisional dataset is implemented for interpolations in the liquid state [11]. As evident from Fig. 10b and previous comparisons, the thermal conductivity of solid tungsten is accurately described, while it is mainly underestimated for liquid tungsten. The deviations increase towards the boiling point but never exceed 20%.

2.5. The mass density

Solid tungsten. The analysis of White and Minges is based on a synthetic dataset constructed from eleven sets of measurements above 300 K and three sets of measurements below 300 K [48]. They provide a least-squares polynomial fit for the linear expansion coefficient $\alpha_l = (1/l_0)(dl/dT)$, where l_0 is the length mea-
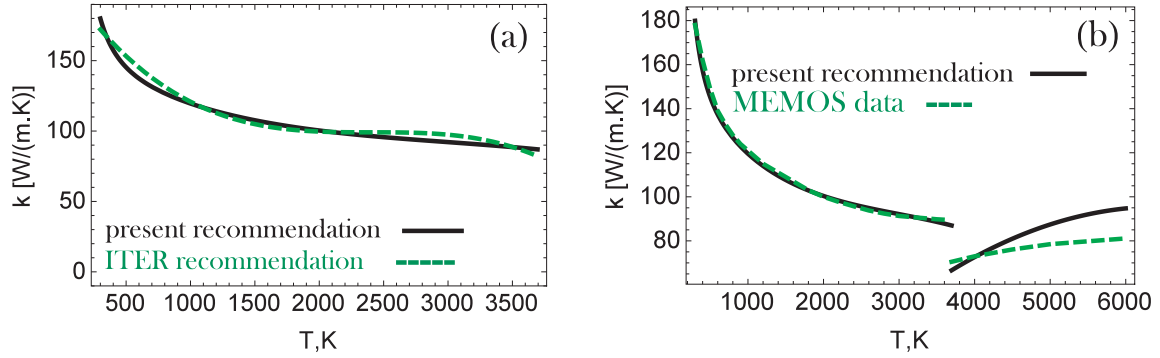
Fig. 10. (a) Comparison of the recommended analytical description of the W thermal conductivity with the ITER database recommendation in the temperature range from 300 to 3695 K. (b) Comparison of the recommended analytical description of the W thermal conductivity with the MEMOS code description in the temperature range from 300 to 6000 K.

sured at the room temperature ($T_0 = 293.15$ K), that is valid from 300 K up to 3500 K. The linear expansion coefficient fit reads as

$$\alpha_l = 3.873 + 2.562 \times 10^{-3}T - 2.8613 \times 10^{-6}T^2 + 1.9862$$
$$\times 10^{-9}T^3 - 0.58608 \times 10^{-12}T^4 + 0.070586 \times 10^{-15}T^5,$$

where α_l is measured in 10^{-6} K^{-1}. These authors only provide tabulated data for the relative change in the linear dimension $\Delta l/l_0 = (l - l_0)/l_0$. An analytical expression for the normalized linear dimension can either be calculated from the relation $l/l_0 = 1 + \int_{T_0}^{T} \alpha_l(T')dT'$ or by least-squares fitting the tabulated data and employing $l/l_0 = 1 + \Delta l/l_0$. Below 3000 K, the average uncertainty was estimated to be 0.5%. The normalized linear dimension fit reads as

$$\frac{l}{l_0} = 1 + 4.64942 \times 10^{-6}(T - T_0) + 2.99884 \times 10^{-11}(T - T_0)^2$$
$$+ 1.95525 \times 10^{-13}(T - T_0)^3.$$

In the case of isotropic thermal expansion for a cubic metal such as tungsten, we have $V/V_0 = (l/l_0)^3$ for the volume expansion. The specific volume fit reads as (1.5% average uncertainty below 3000 K)

$$\frac{V}{V_0} = 1 + 1.4016 \times 10^{-5}(T - T_0) + 4.4004 \times 10^{-11}(T - T_0)^2$$
$$+ 6.3724 \times 10^{-13}(T - T_0)^3.$$

Finally, the dependence of the mass density of solid tungsten on the temperature can be evaluated by employing $\rho_{m0} = 19.25$ g cm^{-3} for the room temperature mass density and $V/V_0 = \rho_{m0}/\rho_m$ as imposed by mass conservation. The *White–Minges fit* reads as

$$\rho_m = 19.25 - 2.66207 \times 10^{-4}(T - T_0) - 3.0595 \times 10^{-9}(T - T_0)^2$$
$$- 9.5185 \times 10^{-12}(T - T_0)^3 \quad 300 \le T(K) \le 3400,$$

where ρ_m is measured in g cm^{-3}.

Liquid tungsten. So far we have employed the Seydel and Fucke measurements [51] for the electrical resistivity and the thermal conductivity of liquid tungsten. It would be consistent to employ the volume expansion data originating from the same experimental group, provided of course that they are reliable. **(i)** Seydel and Kitzel have provided thermal volume expansion data for five refractory metals (Ti, V, Mo, Pd, W) from their melting up to their boiling point [73]. They have successfully fitted the specific volume of tungsten to a quadratic polynomial. The uncertainty in the specific volume was estimated to be $6 - 8$%. The *Seydel–Kitzel fit* reads as

$$\frac{V}{V_0} = 1.18 + 6.20 \times 10^{-5}(T - T_m) + 3.23 \times 10^{-8}(T - T_m)^2,$$

where V_0 is the tungsten specific volume in room temperature. It is worth noting that the Seydel–Kitzel fit has been singled out as the recommended expression in specialized reviews [74]. **(ii)** Hixson and Winkler have measured the specific volume of liquid tungsten in the range $3695 \le T(K) \le 5700$ [28]. They have provided linear expressions for the specific volume as a function of the enthalpy and for the enthalpy as a function of the temperature. Combining their expressions, we acquire the *Hixson–Winkler fit* that reads as (~ 4% uncertainty)

$$\frac{V}{V_0} = 0.83634 + 0.901 \times 10^{-4}T,$$

where V_0 is the tungsten specific volume in room temperature. **(iii)** Kaschnitz, Pottlacher and Windholz have carried out similar measurements without providing fitting expressions [29]. However, the analytical fit of the specific volume as a function of the temperature has been plotted in a figure. We digitized this figure in the temperature range $3695 \le T(K) \le 6000$ with steps of 100 K and we least-square fitted the resulting dataset to a quadratic polynomial. The uncertainty in the specific volume was estimated to be $4 - 7$%. The *Kaschnitz–Pottlacher–Windholz fit* reads as

$$\frac{V}{V_0} = 1.184 + 5.27 \times 10^{-5}(T - T_m) + 1.17 \times 10^{-8}(T - T_m)^2,$$

where again V_0 is the tungsten specific volume in room temperature. The mean value of the absolute relative fitting error is 0.05%. **(iv)** Hüpf et al. have also measured the volume expansion of five refractory liquid metals (V, Nb, Ta, Mo, W) [53]. We note that the authors provided a fit for the quantity D^2/D_0^2 as a function of the temperature, where D denotes the wire diameter. Under rapid heating the melted wire expands solely in the radial direction, which implies that its volume is proportional to the cross-section and thus $V/V_0 = D^2/D_0^2$ [67,75]. The overall measurement uncertainty in the specific volume is expected to be $6 - 8$%. The fitting expression consists of two polynomial branches, but it is continuous at the branch point. The *Hüpf fit* reads as

$$\frac{V}{V_0} = \begin{cases} 0.95062 + 6.344 \times 10^{-5}T & 3695 \le T(K) \le 5000, \\ 1.34989 - 1.0333 \times 10^{-4}T + 1.73957 \times 10^{-8}T^2 & 5000 \\ \le T(K) \le 6000, \end{cases}$$

where again V_0 is the tungsten specific volume in room temperature. The four fits are illustrated in Fig. 11a. It is evident that the Seydel–Kitzel fit greatly overestimates the volume expansion for very high temperatures with the deviations from the other curves starting from 4500 K. The cause of this overestimation was investigated in a seminal paper by Ivanov, Lebedev and Savvatimskii [75]; All the aforementioned experiments were based on the resistive pulse heating technique and the volume expansion measurements were carried out by recording the temporal evolution
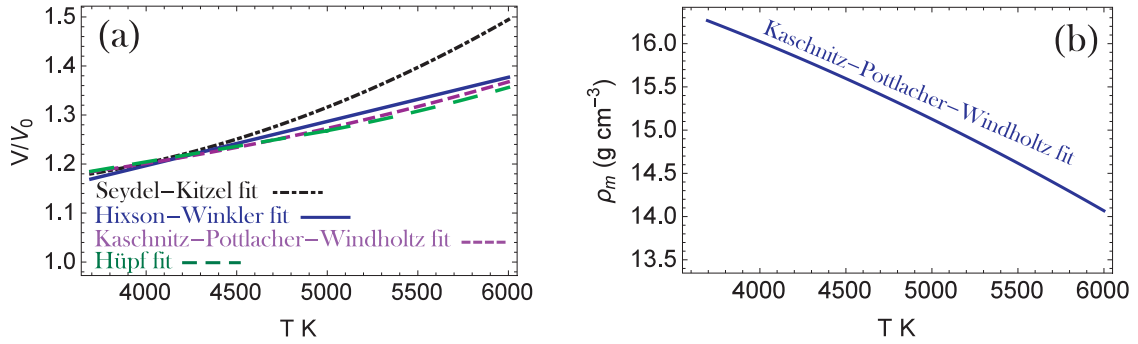
Fig. 11. (a) The liquid tungsten thermal volume expansion in the range $3695 < T(\mathrm{K}) < 6000$ according to four empirical analytical expressions [28,29,53,73]. (b) The mass density of liquid tungsten in the range $3695 < T(\mathrm{K}) < 6000$ according to the Kaschnitz–Pottlacher–Windholz fit [29].

of the shadow the sample produced after illumination with a radiation source either in a dense gas or in a liquid. Only Seydel and Kitzel performed their experiments in water [73]. In the latter case, a vapor layer surrounded the sample with its thickness determined by the sample temperature and its rapid evolution. Since vapor possesses a refractive index smaller than that of water, the vapor layer caused the shadow image to expand and was responsible for the overestimation. The correctness of the other fits was confirmed by the same authors by measurements of the thermal expansion of liquid tungsten with two alternative independent techniques, the capillary method and the probe method [73] ($\sim$5% uncertainty). From Fig. 11a, it is also evident that, close to the melting point, the Hüpf fit deviates from the other curves. Combining the above and considering the more limited temperature range of the Hixson–Winkler fit, we conclude that the Kaschnitz–Pottlacher–Windholz fit is the most appropriate. It is preferable to convert this fit to an analytical expression for the mass density. Using $\rho_{m0} = 19.25\,\mathrm{g\,cm^{-3}}$ for the room temperature mass density of tungsten and $V/V_0 = \rho_{m0}/\rho_m$, we acquire the *Kaschnitz–Pottlacher–Windholz fit* for the mass density

$$\rho_m = 16.267 - 7.679 \times 10^{-4}(T - T_m) - 8.091$$
$$\times 10^{-8}(T - T_m)^2 \quad 3695 \leq T(\mathrm{K}) \leq 6000,$$

where ρ_m is measured in $\mathrm{g\,cm^{-3}}$. This fit is illustrated in Fig. 11. The density of liquid tungsten at the melting point is $\rho_m^l = 16.267\,\mathrm{g\,cm^{-3}}$, which is very close to typical values recommended in handbooks.

Recommended description. In order to complete the description, it is necessary to verify that the White–Minges fit is reliable at high temperatures close to the melting point. Miiller and Cezairliyan had employed a precise high-speed interferometric technique for the measurement of the thermal expansion of tungsten from 1500 K up to the melting point [76]. The maximum uncertainty in the measured linear expansion was estimated to be $\sim$1% at 2000 K and $\sim$2% at 3600 K. From Fig. 12a, it is clear that their experimental results are nearly indistinguishable from the White–Minges fit. Overall, the recommended description comprises of the White–Minges fit in the temperature range $300 < T(\mathrm{K}) < 3695$ and the Kaschnitz–Pottlacher–Windholz fit in the temperature range $3695 < T(\mathrm{K}) < 6000$. See Fig. 12b for an illustration. From the above, we have $\rho_m^s = 17.934\,\mathrm{g\,cm^{-3}}$ and $\rho_m^l = 16.267\,\mathrm{g\,cm^{-3}}$. The resulting discontinuity at the liquid-solid phase transition is $\Delta\rho_m = 1.667\,\mathrm{g\,cm^{-3}}$. As expected we have $\rho_m^s > \rho_m^l$ similar to most metals [50]. It is worth noting that the large relative magnitude of the discontinuity implies a rather large volume expansion during melting compared to other bcc metals [50].

2.6. The surface tension

Significance. The surface tension is a fundamental physical quantity in various plasma-material interaction phenomena that are important for fusion devices: *(i) Droplet generation.* The velocity difference at the interface between the edge plasma and the melt layer leads to the development of the Kelvin–Helmholtz instability and the growth of surface waves whose subsequent breakup can result to metallic droplet ejection into the plasma [77,78]. The surface tension impedes the growth of the K-H instability by providing the restoring force that stabilizes short wavelength perturbations [79]. *(ii) Droplet disintegration.* The shape of charged spherical droplets is subject to distortions due to electrostatic pressure [80]. The surface tension counteracts the electrostatic pressure which tends to rip the droplets apart. The application of the classical Rayleigh linear analysis for metallic droplets embedded in fusion plasmas leads to a threshold radius below which electrostatic disruption occurs and whose value is inversely proportional to the surface tension [81]. *(iii) Melt-layer motion.* Surface tension gradients stemming from surface temperature gradients naturally result to thermo-capillary flows that can influence macroscopic melt-layer motion. Since surface tension enters the mathematical description through the boundary condition that expresses the balance between the tangential hydrodynamic stress and the surface tension gradient, its effect is more transparent when inspecting the Navier–Stokes system within the shallow water approximation, where it contributes a source term proportional to $(\partial\sigma/\partial T)(\nabla T)$ to the non-normal liquid metal velocity components [11].

Liquid metals. Conventional techniques can be utilized for the measurement of the surface tension of liquid metals such as the maximum bubble pressure method, the sessile drop method and the pendant drop - drop weight method [82]. For melts of refractory metals, container-less (or non-contact) methods and particularly levitating drop methods are required in order to eliminate the possibility of chemical reactions between the melt and crucibles or substrates [83–85]. Different variants of the levitating drop method have been developed such as aerodynamic, optical, electrostatic and electromagnetic levitation [84,85]. The experimental results originating from electrostatic levitation measurements are generally considered to be more accurate [83] due to the inherent advantages of this method [85,86]. The electrostatic levitation method is based on lifting a small charged material sample with the aid of electrostatic fields, melting the sample with the aid of lasers, inducing shape oscillations by applying a small amplitude ac modulation to the field, recording the oscillating frequency as well as the amplitude damping of the drop shape profile, which provide the surface tension and the viscosity [86]. It is worth noting that the temperature dependence of the liquid metal surface tension has also been extensively studied because of the
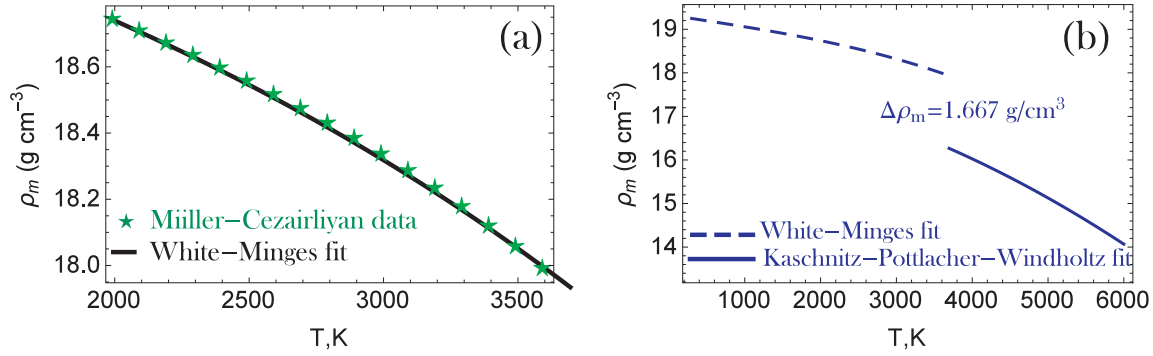
Fig. 12. (a) Comparison of the White–Minges fit close to the tungsten melting point, $2000 < T(K) < 3695$, with the dedicated high temperature measurements of Miiller and Cezairliyan [76]. (b) The complete recommended analytical description of the tungsten mass density from 300 to 6000 K.

Table 3
The surface tension of tungsten at the melting temperature according to dedicated experiments. The dataset of Allen [92] has been corrected for the liquid mass density following Ref. [94], since the exact experimental output in the pendant drop - drop weight method is the ratio σ/ρ_m and the room-temperature tungsten density was employed in the original work.

Investigators	Reference	Year	σ_m (N/m)	Experimental method
Caverly	[91]	1957	2.300	pendant drop - drop weight
Allen	[92]	1963	2.355	pendant drop - drop weight
Martsenyuk et al.	[93]	1974	2.316	pendant drop - drop weight
Vinet et al.	[94]	1993	2.310	pendant drop - drop weight
Paradis et al.	[90]	2005	2.480	electrostatic levitation

aforementioned thermo-capillary Marangoni flows. In general, it is assumed that the dependence of the surface tension of pure liquid metals on the temperature is linear [82,83,85,87]. This linearity is not imposed by generic theoretical arguments, but more likely stems from the limited temperature range of the experiments and the insufficient accuracy of the measurements. The basic constraint imposed by thermodynamics is that the surface tension reduces to zero at the critical point [50]. These remarks imply that the temperature coefficient is always negative; positive values have been measured but - most of the times - they can be attributed to impurity effects or non-equilibrium conditions [50].

Liquid tungsten. Numerous reviews dedicated to experimental measurements of the surface tension of liquid metals can be encountered in the literature [82,83,88,89]. In these compilations, very few data can be found for the surface tension of tungsten at the melting point and no measurements can be found for the temperature dependence of the tungsten surface tension. Fortunately, very recent experiments were carried out by Paradis et al. with the electrostatic levitation method [90]. The surface tension was measured for liquid tungsten barely above the melting point and in the under-cooled phase, $3360 < T(K) < 3700$. The temperature interval of 350 K can be considered as adequate for the determination of the temperature coefficient. A linear fit of the form $\sigma = \sigma_m - \beta(T - T_m)$ provided an accurate description of the data, which - in absence of other measurements - needs to be extrapolated in the entire liquid phase. The *Paradis fit* reads as [90]

$$\sigma = 2.48 - 0.31 \times 10^{-3}(T - T_m)$$

where σ is measured in N/m. The uncertainties in the least square fit coefficients are $\sim 10\%(\sigma_m)$ and $\sim 25\%(\beta)$. The surface tension at the melting point σ_m displays a strong agreement with previous measurements, as seen in Table 3. We shall check how physical is the experimental value of the linear coefficient β by extrapolating at very high temperatures and determining the critical point temperature from $\sigma = 0$. The result is $T_c \simeq 11,700$ K. There is a remarkable agreement with numerous estimates of the tungsten critical point. In particular; the Guldberg rule leads to 12, 277 K, the

Likalter equation of state leads to 12, 466 K, the Goldstein scaling leads to 11, 852 K and dynamic experiments using exploding wires lead on average to 12, 195 K [95].

2.7. The dynamic viscosity

Liquid metals. Conventional experimental techniques can be employed for the measurement of the dynamic viscosity of liquid metals such as the capillary method, the oscillating vessel method, the rotating cylinder method [50,96,97]. For melts of refractory metals, non-contact techniques such as the electrostatic levitation method are preferred due to the high melting temperatures and the enhanced reactivity at elevated temperatures [98,99]. In general, it is assumed that the dependence of the dynamic viscosity of pure liquid metals on the temperature is of the Arrhenius form [50,87], i.e. $\mu(T) = \mu_0 \exp[E_a/(RT)]$ with E_a the activation energy for viscous flow, μ_0 the pre-exponential viscosity and $R = 8.314 \, J/(mol \cdot K)$ the ideal gas constant. It should also be emphasized that, within some limitations, the dynamic viscosity and the surface tension are connected by a rigorous statistical mechanics relation. The Fowler formula for the surface tension of liquids reads as $\sigma(T) = (\pi n^2/8) \int_0^\infty r^4 g(r,T)[d\phi(r,T)/dr]dr$, where $g(r,T)$ is the pair correlation function, $\phi(r,T)$ is the effective pair interaction potential and n is the particle number density [100,101]. The Born–Green formula for the viscosity of liquids reads as $\mu(T) = \sqrt{m/(k_B T)}(2\pi n^2/15) \int_0^\infty r^4 g(r,T)[d\phi(r,T)/dr]dr$, with m the particle atomic mass [102]. Dividing by parts, the so-called Fowler–Born–Green formula emerges, $\mu(T) = (16/15)\sqrt{m/(k_B T)}\sigma(T)$ [103–105]. The fundamental assumptions behind the Fowler formula and the Born–Green formula determine the applicability range of this simple elegant formula [105], which has proved to be very accurate for elemental liquid metals [50].

Liquid tungsten. Numerous works that have reviewed experimental data for the viscosity of liquid metals, elemental but also alloys, can be encountered in the literature [43,87,106–108]. Similar to the case of surface tension, in these compilations, very few data can be found for the viscosity of tungsten at the melt-
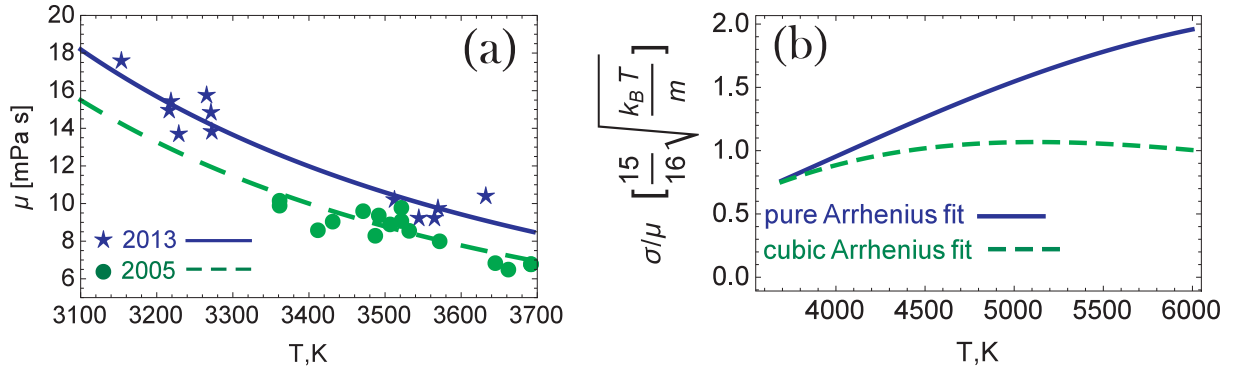
Fig. 13. (a) The viscosity of liquid tungsten in the under-cooled phase; experimental results and Arrhenius least square fits [109,110]. (b) The validity of the Fowler–Born–Green formula across the liquid phase of tungsten adopting the linear expression for the surface tension and either a pure Arrhenius or a cubic Arrhenius expression for the viscosity.

ing point and nearly no measurements for its temperature dependence. The only exception are very recent experiments that were carried out by Ishikawa et al. with the electrostatic levitation method [109,110]. The measurements reported in Ref.[110] will be considered in greater detail, since it has been concluded that the measurements of Ref.[109] were affected by sample positioning forces. In Ref.[110], the viscosity was measured for liquid tungsten in the under-cooled phase, $3155 < T(\mathrm{K}) < 3634$. The temperature interval of $480\,\mathrm{K}$ can be considered as adequate for the determination of the temperature dependence. An Arrhenius fit of the form $\mu = \mu_0 \exp\left[E_a/(RT)\right]$ provided an accurate description of the data, which - in absence of other measurements - needs to be extrapolated in the entire liquid phase. The *Ishikawa fit* reads as [110]

$$\mu = 0.16 \times 10^{-3} \exp\left(3.9713 \frac{T_{\mathrm{m}}}{T}\right),$$

where μ is measured in Pa s. This expression corresponds to an activation energy $E_a = 122 \times 10^3\,\mathrm{J/mol}$ which has been determined by least square fitting with a 20% uncertainty. The extrapolated value of the viscosity at the melting point is $\mu(T_{\mathrm{m}}) = 8.5 \times 10^{-3}\,\mathrm{Pa\,s}$ close to the experimental value $\mu(T_{\mathrm{m}}) = 7.0 \times 10^{-3}\,\mathrm{Pa\,s}$ provided in the literature [87]. Both measurements of Ishikawa et al. [109,110] are illustrated in Fig. 13a together with the least square fitted Arrhenius expressions. In the absence of other experimental results, the Fowler–Born–Green formula provides the only way to cross-check the adopted measurements. In Fig. 13b, the ratio of $\sigma(T)/\mu(T)$, where $\sigma(T)$ follows the Paradis fit and $\mu(T)$ follows the Ishikawa fit, is expressed in units of $(15/16)\sqrt{(k_{\mathrm{B}}T)/m}$ and plotted as a function of the temperature. The quantity does not diverge strongly from unity, especially taking into account the experimental uncertainties and the wide extrapolations in the viscosity as well as the surface tension. It is worth investigating whether fitting expressions other than the pure Arrhenius form can equally fit the experimental data, but provide a better agreement with the Fowler–Born–Green formula. A cubic Arrhenius fit,

$$\mu = 2.76 \times 10^{-3} \exp\left[1.1362 \left(\frac{T_{\mathrm{m}}}{T}\right)^3\right],$$

where μ is measured in Pa s, fulfills these two criteria. It is impossible to determine whether the extrapolated Arrhenius fit for the viscosity or the extrapolated linear fit for the surface tension are responsible for the deviations from the Fowler–Born–Green formula, not to mention that this formula should not be exactly obeyed across the liquid phase. Therefore, we still recommend the use of the pure Arrhenius fit. The aim of this comparison was to highlight the need for tungsten surface tension and viscosity measurements in larger temperature ranges and for temperatures exceeding the melting point.

3. Discussion and summary

3.1. Complications in burning fusion plasma environments

The recommended analytical expressions are nearly exclusively based on experimental results for pure polycrystalline tungsten. Nevertheless, unless rather extreme cases are considered, microstructural details and impurity concentrations should have a negligible influence on the thermophysical properties of interest. Even in the case of pure surface quantities that are very sensitive to adsorbates, such as the surface tension in the liquid phase, the volatility of low-Z contaminants at elevated temperatures guarantees a limited effect. Considering the hostile edge plasma environment of magnetic fusion reactors, it is inevitable that complications arise which should be discussed in further detail. These mainly concern the possible impact of external magnetic fields, plasma contamination, beryllium-tungsten alloying and neutron irradiation.

(a) *Magnetic field effects.* The prominent role of the de-localized valence electrons in charge and heat transport implies that strong external magnetic fields could influence the magnitude and alter the isotropic nature of thermophysical properties such as the thermal conductivity or the electrical resistivity. However, even for high field strengths, magnetic field effects can be expected to be very weak for tungsten, since the mean free paths are much smaller than the Larmor radii due to the enormous density of the scattering centers. Order of magnitude estimates can be performed with the aid of the elementary Drude model, *i.e.* a single particle description with friction described by the relaxation time approximation [60]. The valence electron density is $n_{\mathrm{e}} \simeq 1.3 \times 10^{29}\,\mathrm{m}^{-3}$ and the mean time between collisions is given by $\tau_{\mathrm{e}} = m_{\mathrm{e}}/(n_{\mathrm{e}}e^2\rho_{\mathrm{el}})$, which lead to $\omega_{\mathrm{ce}}\tau_{\mathrm{e}} = B/(en_{\mathrm{e}}\rho_{\mathrm{el}})$, where ω_{ce} denotes the cyclotron frequency of the valence electrons. For $B = 6\,\mathrm{T}$ and room temperature, we have $\omega_{\mathrm{ce}}\tau_{\mathrm{e}} \sim 5 \times 10^{-3}$. Within the Drude model, the relative electrical resistivity increase is $\Delta\rho_{\mathrm{el}}/\rho_{\mathrm{el}} = (\omega_{\mathrm{ce}}\tau_{\mathrm{e}})^2$ [60] which is clearly negligible.

(b) *Plasma contaminants.* As analyzed in the previous section, for high impurity or imperfection concentrations, interaction with defects may dominate the valence electron transport and thus drastically modify quantities such as the thermal conductivity or the electrical resistivity. High hydrogen and helium atom concentrations are unavoidable in the surface proximity of plasma-facing components, owing to the implantation and trapping of the incident plasma ions. It has been documented in the literature that helium bubble and tungsten fuzz formation lead to the degradation of the local thermal properties [111,112], as expected from the porous or fiber-like surface morphology. In particular, recent ther-

mal conductivity measurements for tungsten damaged by high flux - low energy helium plasma revealed a 80% reduction [113]. Such phenomena may have an impact on the PFC power-handling capabilities and more systematic measurements need to be carried out in order to document the extent of the thermally degraded near-surface region. However, they are most likely not relevant for repetitive transient melting events. At elevated temperatures (still well below the melting temperature), trapped gas desorption accompanied by nano-structure annealing [112,114] can be expected to strongly limit the effect of plasma contamination from the beginning of the ELM cycle.

(c) *Be-W alloying effects.* Beryllium erosion from the first wall and its transport to the divertor has been well-understood and documented in JET [115,116]. Moreover, the ITER divertor surface is expected to be covered by a thin Be layer [112]. Under the appropriate plasma conditions (so that significant Be concentrations remain locally deposited) and surface temperatures (so that element inter-diffusion is significant) beryllium-tungsten alloys can form, for instance Be_2W with $T_m \sim 2520\,K$ or $Be_{12}W$ with $T_m \sim 1780\,K$ [112,117–120]. As exhibited by the lower melting points, mixed Be-W materials are characterized by thermophysical properties that strongly depend on the alloy stoichiometry. Optimized conditions for the growth of Be-W alloys might occur near the strike point [121]. Further R&D is necessary to quantify the local extent of Be-W alloy formation. It is evident though that, unless the thickness of the alloy layer is significant, its presence will not be important for thermal or hydrodynamic modelling in spite of the totally different thermophysical properties compared to W. In addition, the Be content will probably vaporize and outgas (surface diffusion and desorption from the molten alloy layers) at temperatures close to the W melting point.

(d) *Neutron irradiation effects.* The penetration depth of neutrons in condensed matter is several orders of magnitude larger than the penetration depth of electrons, ions or photons of comparable incident energy due to the absence of Coulomb interactions with bound electrons and the smallness of the nuclear cross-sections [122]. The penetration depth of fusion ions / electrons in tungsten is $\sim 1 - 10$ nm, whereas the penetration depth of D-T fusion neutrons in tungsten is $\sim 1 - 10$ cm [123]. Thus, neutron-induced damage is much more extended in volume than plasma-induced damage, even when accounting for bulk diffusion. Neutron irradiation can significantly modify the thermophysical properties of tungsten and particularly the thermal conductivity [123–128], as a consequence of atomic displacements (electron-defect interaction term) and nuclear transmutation (electron-phonon interaction term). The strength of this modification depends on the neutron spectrum, the neutron fluence and the irradiation temperature [123]. Unfortunately, experimental works on the subject are still limited [129,130]. The effect of atomic displacements is hard to quantify, especially because of mitigation by annealing at high temperatures. However, a further investigation of the effect of transmutation in the tungsten power handling capabilities is viable. The principal tungsten transmutation products due to bombardment with D-T fusion generated neutrons are rhenium and osmium [131]. At 300 K, the thermal conductivities of W, Re and Os are 174, 47.9 and 87.6 W/(m K), respectively [64]. We shall focus on rhenium owing to its smaller thermal conductivity and its larger solubility limit in tungsten but also because tungsten-rhenium alloys have been extensively studied due to their applications in high temperature thermocouples. The solid solubility limit of Re in W increases with the temperature ($\sim 28\%$ at 2000 K and $\sim 37\%$ at 3300 K) and, apart from the solid solutions, two homogeneous intermetallic phases exist (broad WRe $\sigma-$phase, narrow WRe_3 $\chi-$phase) [132]. Numerous works have measured the temperature dependence of the electrical resistivity and thermal conductivity of pure Re [133–136] as well as W-Re alloys [137–143] in

the solid and liquid phase. Some selected datasets are illustrated in Fig. 14. The generic picture emerging is summarized in the following: (i) As the Re concentration increases, the thermal conductivity of the alloy monotonically decreases. The rate of decrease is rapid up to roughly 10% Re but it saturates around 20%. (ii) In contrast to pure W, the thermal conductivity of solid W-Re alloys is monotonically increasing at elevated temperatures. Consequently, the thermal conductivity deviation from pure W is strongly reduced compared to the room temperature. (iii) In the liquid phase, the thermal conductivity of W-Re alloys is very close to W. In fact, even the differences between pure W and pure Re are very small above the melting points. Overall, W transmutation to Re alone can lead to a drastic reduction of the room temperature thermal conductivity up to $\sim 70\%$ which becomes progressively lower as the temperature increases and eventually vanishes at the W melting point. We point out that transmutation is estimated to be very limited in ITER but is a primary concern for DEMO [144].

To sum up, the thermophysical properties of tungsten are barely affected even by strong fusion-relevant magnetic fields. Plasma contaminants and beryllium-tungsten alloying can substantially alter the W thermophysical properties but only in a relatively thin "unstable" surface layer, which implies that they can be neglected in the modelling of bulk PFCs. We note though that the Be-W mixing depth range is likely comparable to the melt layer depth expected for transient ELM heat loads. It should also be pointed out that the degradation of the thermal properties of such thin layers needs to be considered in the analysis of IR camera measurements [145–148], which might otherwise strongly overestimate the incident plasma heat flux [145]. On the other hand, neutron irradiation can substantially modify the thermophysical properties of W in an extended volume but becomes important for high neutron fluences relevant for DEMO but not for ITER.

3.2. Status of the experimental datasets

As a consequence of its extensive use in high temperature technological applications as well as due to its high melting point and very extended liquid range, pure polycrystalline tungsten can be considered as a standard reference material in the metrology of thermophysical quantities. The development of dynamic pulse calorimetry (starting from the 70s) has allowed for accurate measurements of the latent heat of fusion, the electrical resistivity, the specific isobaric heat capacity, the thermal conductivity and the mass density across the solid and liquid state. The development of levitation calorimetry (starting from the 80s) has allowed for accurate measurements of the surface tension and the dynamic viscosity at the beginning of the liquid state. Hence, it has been possible to provide accurate analytical expressions for the temperature dependence of most properties of interest based solely on experimental data and without the need for any extrapolations. The only exceptions are the surface tension and dynamic viscosity of liquid tungsten, where wide extrapolations had to be carried out beyond the melting point, since the only experimental sources on the temperature dependence referred to under-cooled liquid tungsten specimen. In spite of these limitations, the extrapolated analytical expressions performed very well against constraints imposed by rigorous statistical mechanics relations. Further measurements of the surface tension and viscosity in the unexplored temperature range are certainly desirable, but the proposed expressions are expected to be fairly accurate. Finally, the effects of plasma contamination, impurity alloying and neutron irradiation in the thermophysical properties of tungsten have been relatively poorly investigated. The sparse measurements available only account for a small part of the vast fusion-relevant parameter space, since not only these effects strongly depend on the incident plasma / impurity / neutron energies and fluences but also because they most probably
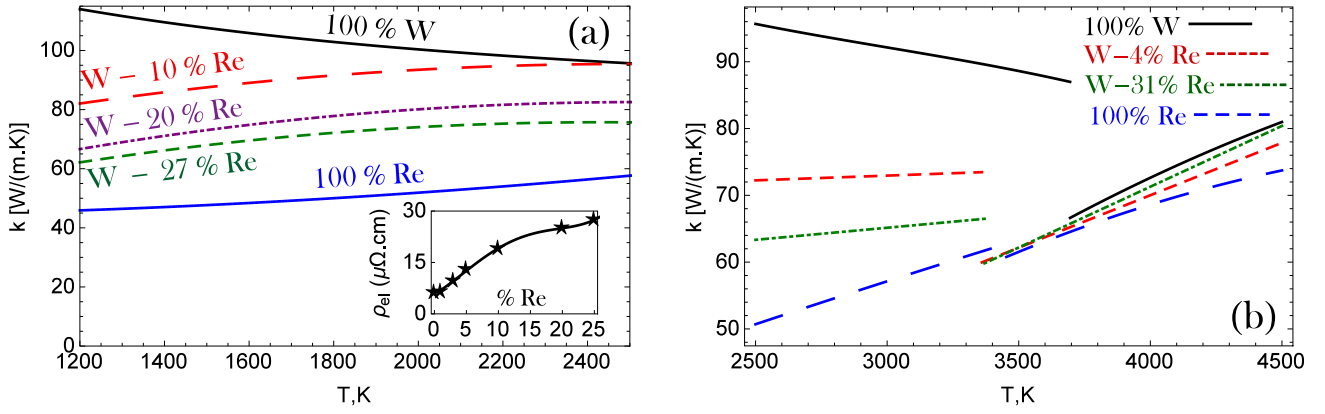
Fig. 14. (a-insert) The room temperature electrical resistivity as a function of the rhenium content for typical W-Re alloys. The measurements are adopted from Refs. [39,141] and the solid curve is drawn to guide the eye. (a-main) The thermal conductivity as a function of the temperature in the 1200 – 2500 K range for pure W and Re as well as several W-Re alloys. Pure rhenium: the recommended dataset of Ho, Powell and Liley [64] in the range 1200 – 2600 K has been employed for quadratic polynomial fits. Rhenium alloys: the measurements of Vertogradskii and Chekhovskoi [137] in the range 1200 – 3000 K have been extracted from plots and fitted to quadratic polynomials. Pure tungsten: the modified Hust–Lankford fit has been employed. (b) The thermal conductivity as a function of the temperature in the 2500 – 4500 K range for pure W and Re as well as several W-Re alloys. Pure rhenium: The tabulated experimental data of Thévenin, Arlés, Boivineau and Vermeulen [136] for the uncorrected electrical resistivity and the thermal volume expansion have been employed for the determination of the electrical resistivity which was then converted to the thermal conductivity with the aid of the Wiedemann–Franz law. The resulting dataset has been fitted with quadratic polynomials in the temperature ranges 2500 – 3453 K (solid) and 3453 – 4500 K (liquid). Rhenium alloys: Linear fits to the thermal conductivity measurements of Seifter, Didoukh and Pottlacher [140] in the temperature range 2500 – 4400 K were employed. The alloy melting ranges are 3325 – 3395 K for W–4% Re and 3319 – 3421 K for W–31% Re. Pure tungsten: the recommended analytical description (the modified Hust–Lankford fit for the solid state and the Seydel–Fucke fit for the liquid state) has been employed.

operate synergetically. However, recent experiments have demonstrated that these effects can severely degrade the power handling capabilities of tungsten. Further experiments in material testing facilities are certainly required in order to evaluate the consequences for ITER and to assess the suitability of tungsten as a plasma-facing component in future fusion reactors.

3.3. Recommended analytical expressions

The thermophysical properties analyzed in this work constitute input for simulations of the thermal and hydrodynamic response of tungsten plasma-facing components, dust and droplets to incident plasma particle and heat fluxes. For this reason, in this concluding paragraph, it was judged to be more practical and convenient for the specialized reader that we simply gather the recommended analytical expressions for the temperature dependence of the thermophysical properties of pure solid and liquid tungsten. Before proceeding, it is worth mentioning that the melt layer motion code MEMOS [12,46] and the dust dynamics code MIGRAINe [15,149] have already been updated following the present recommendations.

For the **latent heat of fusion**, we recommend the typical literature value of

$$\Delta h_f = 52.3,$$

where Δh_f is measured in kJ/mol. For the **electrical resistivity**, we recommend the White–Minges fit in the temperature range $100 \leq T(\text{K}) \leq 3695$ and the Seydel–Fucke fit in the temperature range $3695 \leq T(\text{K}) \leq 6000$,

$$\rho_{el}(T) = \begin{cases} -0.9680 + 1.9274 \times 10^{-2}T + 7.8260 \times 10^{-6}T^2 - 1.8517 \\ \times 10^{-9}T^3 + 2.0790 \times 10^{-13}T^4 \quad 100 \leq T(\text{K}) \leq 3695, \\ 135 - 1.855 \times 10^{-3}(T - T_m) + 4.420 \\ \times 10^{-6}(T - T_m)^2 \quad 3695 \leq T(\text{K}) \leq 6000, \end{cases}$$

where ρ_{el} is measured in $10^{-8}\,\Omega\text{m}$ or in $\mu\Omega\text{cm}$. For the **specific isobaric heat capacity**, we recommend the White–Minges fit in the temperature range $300 \leq T(\text{K}) \leq 3080$, the Wilthan et al. fit in the temperature range $3080 \leq T(\text{K}) \leq 3695$ and the Wilthan et al. value

in the temperature range $T(\text{K}) \geq 3695$,

$$c_p(T) = \begin{cases} 21.868372 + 8.068661 \times 10^{-3}T - 3.756196 \times 10^{-6}T^2 \\ +1.075862 \times 10^{-9}T^3 + \dfrac{1.406637 \times 10^4}{T^2} \quad 300 \\ \leq T(\text{K}) \leq 3080 \\ 2.022 + 1.315 \times 10^{-2}T \quad 3080 \leq T(\text{K}) \leq 3695 \\ 51.3 \quad T(\text{K}) \geq 3695 \end{cases}$$

where c_p is measured in J/(mol K). For the **thermal conductivity**, we recommend the modified Hust–Lankford fit in the temperature range $300 < T(\text{K}) < 3695$ and the Seydel–Fucke fit in the temperature range $3695 < T(\text{K}) < 6000$,

$$k(T) = \begin{cases} 149.441 - 45.466 \times 10^{-3}T + 13.193 \times 10^{-6}T^2 - 1.484 \\ \times 10^{-9}T^3 + \dfrac{3.866 \times 10^6}{T^2} \quad 300 \leq T(\text{K}) \leq 3695 \\ 66.6212 + 0.02086(T - T_m) - 3.7585 \\ \times 10^{-6}(T - T_m)^2 \quad 3695 \leq T(\text{K}) \leq 6000, \end{cases}$$

where k is measured in W/(m K). For the **mass density**, we recommend the White–Minges fit in the temperature range $300 < T(\text{K}) < 3695$ and the Kaschnitz–Pottlacher–Windholz fit in the temperature range $3695 < T(\text{K}) < 6000$,

$$\rho_m(T) = \begin{cases} 19.25 - 2.66207 \times 10^{-4}(T - T_0) - 3.0595 \\ \times 10^{-9}(T - T_0)^2 - 9.5185 \times 10^{-12}(T - T_0)^3 \quad 300 \\ \leq T(\text{K}) \leq 3695, \\ 16.267 - 7.679 \times 10^{-4}(T - T_m) - 8.091 \\ \times 10^{-8}(T - T_m)^2 \quad 3695 \leq T(\text{K}) \leq 6000, \end{cases}$$

where ρ_m is measured in g cm^{-3} and $T_0 = 293.15$ K. For the **surface tension**, we recommend the extrapolated linear Paradis fit

$$\sigma(T) = 2.48 - 0.31 \times 10^{-3}(T - T_m) \quad T(\text{K}) \geq 3695,$$

where σ is measured in N/m. For the **dynamic viscosity**, we recommend the extrapolated Arrhenius Ishikawa fit

$$\mu(T) = 0.16 \times 10^{-3} \exp\left(3.9713\frac{T_m}{T}\right) \quad T(\text{K}) \geq 3695,$$

where μ is measured in Pa s.

Acknowledgments

References

[1] R.A. Pitts, A. Kukushkin, A. Loarte, A. Martin, et al., *Phys. Scr.* T138 (014001) (2009).
[2] R.A. Pitts, S. Carpentier, F. Escourbiac, T. Hirai, et al., J. Nucl. Mater. 438 (S48) (2013).
[3] G. Pintsuk, Compr. Nucl. Mater. 4 (551) (2012).
[4] M. Rieth, S.L. Dudarev, S.M.G. de Vicente, J. Aktaa, et al., *J. Nucl. Mater.* 432 (482) (2013).
[5] C. Linsmeier, M. Rieth, J. Aktaa, T. Chikada, et al., Nucl. Fusion 57 (092007) (2017).
[6] I. Smid, M. Akiba, G. Vieider, L. Plöchl, J. Nucl. Mater. 258–263 (160) (1998).
[7] J.W. Davis, V.R. Barabash, A. Makhankov, L. Plöchl, K.T. Slattery, J. Nucl. Mater. 258–263 (308) (1998).
[8] V. Barabash, et al., J. Nucl. Mater. 367–370 (21) (2007).
[9] J.W. Coenen, V. Philipps, S. Brezinsek, B. Bazylev, et al., Nucl. Fusion 51 (083008) (2011).
[10] J.W. Coenen, G. Arnoux, B. Bazylev, G.F. Matthews, et al., Nucl. Fusion 55 (023010) (2015).
[11] B. Bazylev, H. Wuertz, J. Nucl. Mater. 307–211 (69) (2002).
[12] B. Bazylev, G. Janeschitz, I. Landman, S. Pestchanyi, et al., Fusion Eng. Des. 83 (1077) (2008).
[13] G. Miloshevsky, A. Hassanein, Nucl. Fusion 54 (043016) (2014).
[14] S.I. Krasheninnikov, R.D. Smirnov, D.L. Rudakov, Plasma Phys. Control. Fusion 53 (083001) (2011).
[15] L. Vignitchouk, P. Tolias, S. Ratynskaia, Plasma Phys. Control. Fusion 56 (095005) (2014).
[16] L. Vignitchouk, S. Ratynskaia, P. Tolias, Plasma Phys. Control. Fusion 59 (104002) (2017).
[17] S. Ratynskaia, P. Tolias, I. Bykov, D. Rudakov, et al., Nucl. Fusion 56 (066010) (2016).
[18] I. Egry, A. Diefenbach, W. Dreier, J. Piller, Int. J. Thermophys. 22 (569) (2001).
[19] T. Ishikawa, J.T. Okada, P.-F. Paradis, Y. Watanabe, Jpn. J. Appl. Phys. 50 (11RD03) (2011).
[20] S.V. Lebedev, A.I. Savvatimskii, Y.B. Smirnov, High Temp. (USSR) 9 (578) (1971).
[21] M.M. Martynyuk, I. Karimkhodzhaev, V.I. Tsapkov, Sov. Phys. Tech. Phys. 19 (1458) (1975).
[22] J.W. Shaner, G.R. Gathers, C. Minichino, High Temp. High Press. 8 (425) (1976).
[23] U. Seydel, H. Bauhof, W. Fucke, H. Wadle, High Temp. High Press. 11 (635) (1979).
[24] D.W. Bonnell, et al., *Materials Measurements*, in: J.R. Manning (Ed.), 1983. NBS Internal Report 83–2772.
[25] E. Arpaci, M.G. Frohberg, Z. Metallkde. 75 (614) (1984).
[26] A. Berthault, L. Arles, J. Matricon, Int. J. Thermophys. 7 (167) (1986).
[27] V.N. Senchenko, M.A. Sheindlin, High Temp. (USSR) 25 (364) (1987).
[28] R.S. Hixson, M.A. Winkler, Int. J. Thermophys. 11 (709) (1990).
[29] E. Kaschnitz, G. Pottlacher, L. Windholz, High Press. Res. 4 (558) (1990).
[30] J.L. McClure, A. Cezairliyan, Int. J. Thermophys. 14 (449) (1993).
[31] G. Pottlacher, E. Kaschnitz, H. Jäger, J. Non-Cryst. Solids 156–151 (374) (1993).
[32] N.I. Kuskova, S.I. Tkachenko, S.V. Koval, Int. J. Thermophys. 19 (341) (1998).
[33] P. Gustafson, Int. J. Thermophys. 6 (395) (1985).
[34] G. Grimvall, M. Thiessen, A.F. Guillermet, Phys. Rev. B 36 (7816) (1987).
[35] A.T. Dinsdale, CALPHAD 15 (317) (1991) 419–420.
[36] E. Lassner, W.-D. Schubert: Tungsten: Properties, Chemistry, Technology of the Element, Alloys, and Chemical Compounds, Springer, Berlin, 1999, pp. 30–34.
[37] D.R. Lide, CRC Handbook of Chemistry and Physics, CRC Press, Boca Raton, 2004, pp. 12.219–12.220.
[38] W. Martienssen, H. Warlimont, Springer Handbook of Condensed Matter and Materials Data, Springer, Berlin, 2005, pp. 114–117.
[39] F. Cardarelli, Materials Handbook: A Concise Desktop Reference, Springer-Verlag, London, 2008, pp. 267–270.
[40] I.L. Shabalin, Ultra-high Temperature Materials I, Springer, Dordrecht, 2014, pp. 238–241.
[41] C. Cagran, G. Pottlacher, Dynamic pulse calorimetry - thermophysical properties of solid and liquid metals and alloys, in: M.E. Brown, P.K. Gallagher (Eds.), *Handbook of Thermal Analysis and Calorimetry Vol. 5: Recent Advances, Techniques and Applications*, Elsevier, Amsterdam, 2005, pp. 333–334.
[42] D.R. Stull, G.C. Sinke, Thermodynamic Properties of the Elements, American Chemical Society, Washington, 1956, pp. 212–213.
[43] G.V. Samsonov, Handbook of the Physicochemical Properties of the Elements, Plenum, New York, 1968, pp. 250–251.
[44] G. Grimvall, Thermophysical Properties of Materials, Elsevier, Amsterdam, 1999. Ch. 12

[45] M.E. Glicksman, Principles of Solidification, Springer, New York, 2011, pp. 21–23.
[46] E. Thorén, B. Bazylev, S. Ratynskaia, P. Tolias, et al. Phys. Scr.(submitted).
[47] P.D. Desai, T.K. Chu, H.M. James, C.Y. Ho, J. Phys. Chem. Ref. Data 13 (1069) (1984) 1091–1095.
[48] G.K. White, M.L. Minges, Int. J. Thermophys. 18 (1269) (1997).
[49] L. Vignitchouk, Modelling the Multifaceted Physics of Metallic Dust and Droplets in Fusion Plasmas, KTH Stockholm, 2016 PhD Thesis.
[50] T. Iida, R. Guthrie, The Thermophysical Properties of Metallic Liquids Volume 1: Fundamentals, Oxford University Press, Oxford, 2015. Ch. 3,6,7,9.
[51] U. Seydel, W. Fucke, J. Phys. F 10 (L203) (1980).
[52] B. Wilthan, C. Cagran, G. Pottlacher, Int. J. Thermophys. 26 (1017) (2005).
[53] T. Hüpf, C. Cagran, G. Lohöfer, G. Pottlacher, J. Phys. Conf. Ser. 98 (062002) (2008).
[54] T. Hüpf, C. Cagran, G. Pottlacher, EPJ Web Conf. 15 (01018) (2011).
[55] M.W. Chase, NIST-JANAF thermochemical tables (fourth edition), J. Phys. Chem. Ref. Data Monogr. 9 (1) (1998) 1925–1931.
[56] http://webbook.nist.gov.
[57] G.K. White, S.J. Collocott, J. Phys. Chem. Ref. Data 13 (1251) (1984).
[58] I. Barin, Thermochemical Data of Pure Substances, VCH, Weinheim, 1995, pp. 1782–1785.
[59] Y.S. Touloukian, E.H. Buyco, Thermophysical Properties of Matter - The TPRC Data Series - Vol.4 Specific Heat - Metallic Elements and Alloys, Plenum, New York, 1971, pp. 263–267.
[60] A.A. Abrikosov, Fundamentals of the Theory of Metals, Elsevier, Amsterdam, 1988. Ch. 3,4,5.
[61] C. Kittel, Introduction to Solid-State Physics, John Wiley & Sons, New Jersey, 2005. Ch. 5,6.
[62] F. Seitz, The Modern Theory of Solids, McGraw-Hill, New York, 1940. Ch. IV.
[63] C.Y. Ho, R.W. Powell, P.E. Liley, J. Phys. Chem. Ref. Data 1 (279) (1972) 408–409.
[64] C.Y. Ho, R.W. Powell, P.E. Liley, J. Phys. Chem. Ref. Data 3 (1974) 689–704. Suppl. 1.
[65] J.G. Hust, A.B. Lankford, Thermal Conductivity of Aluminum, Copper, Iron and Tungsten for Temperatures from 1 K to the Melting Point, U. S. Department of Commerce, Boulder, 1984, pp. 199–256. NBS Internal Report 84-3007.
[66] K.C. Mills, B.J. Monaghan, B.J. Keene, Int. Mater. Rev. 41 (209) (1996).
[67] M. Boivineau, G. Pottlacher, Int. J. Mater. Prod. Tec. 26 (217) (2006).
[68] G. Pottlacher, J. Non-Cryst. Solids 250–252 (177) (1999).
[69] H. Hess, A. Kloss, A. Rakhel, H. Schneidenbach, Int. J. Thermophys. 20 (1279) (1999).
[70] A.V. Grosse, J. Inorg. Nucl. Chem. 28 (795) (1966).
[71] A.V. Grosse, J. Inorg. Nucl. Chem. 28 (803) (1966).
[72] Y.S. Touloukian, R.W. Powell, C.Y. Ho, P.G. Klemens, Thermophysical Properties of Matter - The TPRC Data Series - Vol.1 Thermal Conductivity - Metallic Elements and Alloys, Plenum, New York, 1970, pp. 415–428.
[73] U. Seydel, W. Kitzel, J. Phys. F 9 (L153) (1979).
[74] G.R. Gathers, Rep. Prog. Phys. 49 (341) (1986).
[75] V.V. Ivanov, S.V. Lebedev, A.I. Savvatimskii, J. Phys. F 14 (1641) (1984).
[76] A.P. Miiller, A. Cezairliyan, Int. J. Thermophys. 12 (643) (1991).
[77] B. Bazylev, G. Janeschitz, I. Landman, A. Loarte, et al., Fusion Eng. Des. 84 (441) (2009).
[78] G. Miloshevsky, A. Hassanein, Nucl. Fusion 54 (033008) (2014).
[79] G. Miloshevsky, A. Hassanein, Nucl. Fusion 50 (115005) (2010).
[80] C.A. Morrison, R.P. Leavitt, D.E. Wortman, J. Fluid Mech. 104 (295) (1981).
[81] M. Coppins, Phys. Rev. Lett. 104 (065003) (2010).
[82] B.J. Keene, Int. Mater. Rev. 38 (157) (1993).
[83] K.C. Mills, Y.C. Su, Int. Mater. Rev. 51 (329) (2006).
[84] I. Egry, E. Ricci, R. Novakovic, S. Ozawa, Adv. Colloid Interface Sci. 159 (198) (2010).
[85] P.-F. Paradis, T. Ishikawa, G.-W. Lee, D. Holland-Moritz, J. Brillo, W.-K. Rhim, J.T. Okada, Mater. Sci. Eng. R Rep. 76 (1) (2014).
[86] W.-K. Rhim, K. Ohsaka, P.-F. Paradis, R.E. Spjut, Rev. Sci. Intrum. 70 (2796) (1999).
[87] T. Iida, R. Guthrie, The Thermophysical Properties of Metallic Liquids Volume 2: Predictive Models, Oxford University Press, Oxford, 2015. Ch. 14,15,17.
[88] O. Flint, J. Nucl. Mater. 16 (233) (1964).
[89] D.W.G. White, Metall. Rev. 13 (73) (1968).
[90] P.-F. Paradis, T. Ishikawa, R. Fujii, S. Yoda, Appl. Phys. Lett. 86 (041901) (2005).
[91] A. Calverley, Proc. Phys. Soc. 70B (1040) (1957).
[92] B.C. Allen, Trans. AIME 227 (1175) (1963).
[93] P.S. Martsenyuk, Y.N. Ivashchenko, V.N. Eremenko, High Temp. 12 (1310) (1974).
[94] B. Vinet, J.P. Garandet, L. Cortella, J. Appl. Phys. 73 (3830) (1993).
[95] H. Hess, Phys. Chem. Liq. 30 (251) (1995).
[96] R.F. Brooks, A.T. Dinsdale, P.N. Quested, Meas. Sci. Technol. 16 (354) (2005).
[97] J. Cheng, J. Gröbner, N. Hort, K.U. Kainer, R. Schmid-Fetzer, Meas. Sci. Technol. 25 (062001) (2014).
[98] T. Ishikawa, P.-F. Paradis, T. Itami, S. Yoda, J. Chem. Phys. 118 (7912) (2003).
[99] T. Ishikawa, P.-F. Paradis, J.T. Okada, Y. Watanabe, Meas. Sci. Technol. 23 (025305) (2012).
[100] R.H. Fowler, Proc. R. Soc. A 159 (229) (1937).
[101] J.G. Kirkwood, F.P. Buff, J. Chem. Phys. 17 (338) (1949).
[102] M. Born, H.S. Green, Proc. R. Soc. A 190 (455) (1947).
[103] I. Egry, Scr. Metall. Mater. 26 (1349) (1992).
[104] I. Egry, G. Lohöfer, S. Sauerland, J. Non-Cryst. Solids 156–158 (830) (1993).

[105] I. Egry, Scr. Metall. Mater. 28 (1273) (1993).
[106] L. Battezzati, A.L. Greer, Acta Metall. 37 (1791) (1989).
[107] R.P. Chhabra, D.K. Sheth, Z. Metallkd. 81 (264) (1990).
[108] T. Iida, R. Guthrie, M. Isac, N. Tripathi, Metall. Mater. Trans. B 37 (403) (2006).
[109] P.-F. Paradis, T. Ishikawa, S. Yoda, J. Appl. Phys. 97 (106101) (2005).
[110] T. Ishikawa, P.-F. Paradis, J.T. Okada, M.V. Kumar, Y. Watanabe, J. Chem. Thermodyn. 65 (1) (2013).
[111] S. Kajita, S. Takamura, N. Ohno, D. Nishijima, et al., Nucl. Fusion 47 (1358) (2007).
[112] Y. Ueda, J.W. Coenen, G. De Temmerman, R.P. Doerner, et al., Fusion Eng. Des. 89 (901) (2014).
[113] S. Cui, M. Simmonds, W. Qin, F. Ren, et al., J. Nucl. Mater. 486 (267) (2017).
[114] G. De Temmerman, K. Bystrov, R.P. Doerner, L. Marot, et al., J. Nucl. Mater. 438 (S78) (2013).
[115] S. Brezinsek, A. Widdowson, M. Mayer, V. Philipps, et al., Nucl. Fusion 55 (063021) (2015).
[116] X. Litaudon, et al., Nucl. Fusion 57 (102001) (2017).
[117] R.P. Doerner, J. Nucl. Mater. 363–365 (32) (2007).
[118] M.J. Baldwin, R.P. Doerner, D. Nishijima, D. Buchenauer, et al., J. Nucl. Mater. 363–365 (1179) (2007).
[119] G. Federici, R. Doerner, P. Lorenzetto, V. Barabash, Compr. Nucl. Mater. 4 (621) (2012).
[120] S. Brezinsek, J.W. Coenen, T. Schwarz-Selinger, K. Schmid, et al., Nucl. Fusion 57 (116041) (2017).
[121] J.N. Brooks, J.P. Allain, J. Nucl. Mater. 390–391 (123) (2009).
[122] H. Schopper (Ed.), Low Energy Neutrons and Their Interaction with Nuclei and Matter. Part 1, Springer-Verlag, Berlin, 2000.
[123] C. Linsmeier, B. Unterberg, J.W. Coenen, R.P. Doerner, et al., Nucl. Fusion 57 (092012) (2017).
[124] V. Barabash, G. Federici, M. Rödig, L.L. Snead, C.H. Wu, J. Nucl. Mater. 283–287 (138) (2000).
[125] V. Barabash, G. Federici, J. Linke, C.H. Wu, J. Nucl. Mater. 313–316 (42) (2003).
[126] A. Hasegawa, M. Fukuda, S. Nogami, K. Yabuuchi, Fusion Eng. Des. 89 (1568) (2014).
[127] J.W. Coenen, S. Antusch, M. Aumann, W. Biel, et al., Phys. Scr. T167 (014002) (2016).
[128] Y. Ueda, K. Schmid, M. Balden, J.W. Coenen, et al., *Nucl. Fusion* 57 (092006) (2017).
[129] M. Fujitsuka, B. Tsuchiya, I. Mutoh, T. Tanabe, T. Shikama, J. Nucl. Mater. 283–287 (1148) (2000).
[130] T. Tanno, A. Hasegawa, J.C. He, M. Fujiwara, et al., J. Nucl. Mater. 386–388 (218) (2009).
[131] L.R. Greenwood, F.A. Garner, J. Nucl. Mater. 212–215 (635) (1994).
[132] F. Predel, Phase Equilibria, Crystallographic and Thermodynamic Data of Binary Alloys, Springer-Verlag, Berlin, 2016.
[133] G. Pottlacher, T. Neger, H. Jäger, Int. J. Thermophys. 7 (149) (1986).
[134] L.A. Dolomanov, K.S. Kovalev, S.V. Lebedev, A.I. Savvatimskii, High Temp. 26 (3591) (1988).
[135] R.S. Hixson, M.A. Winkler, Int. J. Thermophys. 13 (477) (1992).
[136] T. Thévenin, L. Arlés, M. Boivineau, J.M. Vermeulen, Int. J. Thermophys. 14 (441) (1993).
[137] V.A. Vertogradskii, V.Y. Chekhovskoi, High Temp. 10 (893) (1972).
[138] A.V. Logunov, A.I. Kovalev, High Temp.-High Press. 5 (625) (1973).
[139] A. Cezairliyan, A.P. Miiller, Int. J. Thermophys. 6 (191) (1985).
[140] A. Seifter, V. Didoukh, G. Pottlacher, Int. J. Thermophys. 20 (1237) (1999).
[141] K.M. Zwilsky, ASM Handbook Volume 2. Properties and Selection: Nonferrous Alloys and Special-Purpose Materials, ASM International, USA, 1990, pp. 1761–1766.
[142] O. Madelung, G.K. White, Thermal Conductivity of Pure Metals and Alloys, Springer-Verlag, Berlin, 1991, pp. 256–258.
[143] T. Tanabe, C. Eamchotchawalit, C. Busabok, S. Taweethavorn, et al., Mater. Lett. 57 (2950) (2003).
[144] H. Bolt, V. Barabash, G. Federici, J. Linke, A. Loarte, J. Roth, K. Sato, J. Nucl. Mater. 307–311 (43) (2002).
[145] A.W. Leonard, A. Herrmann, K. Itami, J. Lingertat, et al., J. Nucl. Mater. 266–269 (109) (1999).
[146] P. Andrew, J.P. Coad, Y. Corre, T. Eich, et al., J. Nucl. Mater. 337–339 (99) (2005).
[147] T. Eich, P. Andrew, A. Herrmann, W. Fundamenski, et al., Plasma Phys. Control. Fusion 49 (573) (2007).
[148] J. Gaspar, F. Rigollet, J.-L. Gardarein, C.L. Niliot, Y. Corre, Int. J. Heat Mass Transf. 56 (147) (2013).
[149] S. Ratynskaia, L. Vignitchouk, P. Tolias, I. Bykov, et al., Nucl. Fusion 53 (123002) (2013).